Attempt to Construct an Alternative Formation Theory of Beat Applied to the Pendelloesung Beat and Proposal of its Confirmatory Experiments at Low Temperatures

Tetsuo. Nakajima

●Abstract

An alternative theory of beat, in which a variation of the intensity of a composite wave is formed from definite distinct waves of which more than two have different frequencies is constructed. It is applied to Pendelloesung beat (hereafter, abbreviated as PB) as an apt example. PB has been observed only in some light elements (below the atomic number 32) by using rather hard X-rays up to 60keV above the room temperatures. These observations for the formation of PB support the view that the recoil energy loss plays the essentially important role in beat production by the superposition of the photons with the reduction of the momentum. The Bragg law for the reduction of the momentum by the recoil is derived based upon the corpuscular character of the light and the principle of the equipartition of the recoil energy over all the atoms in the crystal. The application of the Bragg law, to the superposition of the expected value of the even or odd time multi-reflex photons (taken by the binomial distribution as stochastic events) forms the two types of the transmitted or diffracted PB, respectively. The law predicts two types of the prominently positive projecting peaks at half wave at even times of π and the plus or minus projecting peaks at odd times of π , according to the multiplicity factor of the reflection, exist as pulsations of bare PB from AM by cosec $\Delta\omega t$ in the basic bare envelope curve. It turns out that the AM effect of the binomial distribution on bare PB makes all of the peaks contracted as if it is erased, and makes the intense collimated photon flux follow as the Borrmann effect. It is proposed this review can be confirmed experimentally by testing the prediction that the integrated reflection intensity of PB fades into quantum PB as a limit near 0K by a reduction of the recoil reflections due to the enhancement of the crystal rigidity with decreasing temperature.

●キーワード

Pendelloesung beat, X-ray diffraction, Recoil reflection, Recoil-free reflection, Binomial distribution

※2004年 9 月 1 日受理(紀要編集委員会)

I. Introduction

In this work, an alternative theory of the beat, in which a variation of the intensity of a composite wave is formed from the superposition of the definite distinct waves of which more than two have slightly different frequencies, is constructed based on using a modified Bragg law and the principle of the equipartition of the recoil energy. It is applied to PB as an archetypal example.

Since the observation of the equal thickness interference fringe in Si, LiF and quartz[1], PB has been observed in many types of the crystals as listed in Table I. These results are generally characterized by the following conditions: *firstly*, the crystals exhibiting PB are distributed across the light elements and for less than one third of all the elements in the periodic table from carbon with Z=6 to Germanium with Z=32 in Table I. See also Fig.1, in which PB is shown to be observed at most within a parallelogram *abcd. Secondly*, all of the examples of PB have been observed above the room temperature and up to near the Debye temperature Θ_D.[16] This means that PB has appeared only in the low Z nonrigid crystals that favor recoil reflection. As is well known, the discovery of the Moessbauer effect (ME)[17-19] revealed a temperature effect,[20] showing that at lower temperatures, the crystal becomes more rigid as confirmed through the microscopic phenomenon of ME. As a result, the effective resonance absorption cross section increases abruptly below about 150K as shown in Fig 2.[17, 20] *Thirdly*, the available X-ray energy E_0 ranges from 10keV to 60keV (see in Fig. 1), which greatly outweighs high values of E_C in the exponent defined by

$$2M=(E_0 \sin\theta_B/E_C)^2 \Phi(t) \qquad (1)$$

in the Debye-Waller (D-W) factor of $D=\exp(-2M)$ (Table I).[21] Here, $\Phi(t)=1+4t^2\int_0^{1/t} ydy/(e^y-1)$ where $t=T/\Theta_D$ and T is the absolute temperature. *Finally*, in these cases, the Bragg angle of θ_B becomes small but the high recoil energy E_R of a single atom by absorption or emission in the reflection of the photon is lost, independent of θ_B, which distributes up to the high value of 161meV from 0.74meV at most (Fig. 1). From these observations, preferred path for the formation of PB is from the recoil X-ray reflection.

From the old quantum theory, new types of the beats are deduced from the superposition of the multiple transmitted and diffracted X-ray photons based upon the supporting experimental factor, without employing the commonly used dynamical theory of X-ray diffraction (DTXD). The contraction of the momentum due to the recoil energy loss in X-ray reflections could make a novel offer to form PB, which varies in the intensity of composite waves as the *beats* formed from the superposition of the multiple distinct waves with successively slightly different frequencies. Experiments to confirm these reductions that are closely related to the role of the recoil reflection as an origin of PB are proposed. These experiments would search for a reverse of the temperature effect in ME[20] that the integrated intensity of PB due to the recoil reflection fades into quantum PB as a limit at 0K by the enhancement of the crystal rigidity with the decreasing temperatures.

II. On the compensation of the recoil energy by the partial charge of all atoms in the crystal based on the principle of the equipartition of it

It has been shown that ME with extremely high energy resolution of $\Delta E/E_0 \cong 3.59\cdot10^{-10}$ for ^{191}Ir[17-19] and $4.67\cdot10^{-13}$ for ^{14}Fe[22] can be achieved by the turntable effect due to the Doppler effect[20] in the resonance absorption

and emission of γ-rays of the nuclei bound in the crystal. This effect outweighs the recoil energy E_R (keV) per a single radioactive atom defined by (Appendix (App) I and Fig. 1),

$$E_R = (1/2m)\cdot(E_0/c)^2, \tag{2}$$

where c is the velocity of light. There exists an energy deficit of $2E_R$ between the absorption and emission of γ-ray in ME. If all of constituent atoms are held in the lattice by tightly binding forces, the single free atomic mass m in eq. (2) should be replaced with Nm for the whole lattice, based upon the principle of the equipartition of the recoil energy loss due to the crystal rigidity (App I). Since N might be typically estimated to range from 10^{10} to 10^{20} atoms, E_R in eq. (2) is reduced by a factor of 10^{-10} to 10^{-20}, with the important result that approximately, $E_R / E_0 \cong 0$, as follows[23, 24]

$$E_R(keV) = \frac{E_0^2}{2Nmc^2} \cong 5.37\cdot(10^{-20}\sim 10^{-30})\cdot\frac{E_0^2(keV)^2}{M_a(kg/mol)}, \tag{3}$$

where m is equal to the quotient of the atomic weight M_a divided by the Avogadro's number N_A. The value of M_a approximately ranges from 10^{-3} to 10^{-1}kg/mol.

As is well known in terms of *cold shortness* or *brittleness*, the rigidity of the crystal is enhanced at low temperatures and therefore, the absorption cross section of ^{191}Ir in Fig. 2 steeply increases below about 150K in ME.[17, 20] It is therefore understood that the temperature change of the elastic constants could be determined from the microscopic phenomena of ME. The temperature effect[20] has been introduced as the D-W factor based on the Debye heat capacity formula by many contributors.[25-28]

The number of N in eq. (3) accidentally comes from the sample size. Unlike ME, the appropriate reduction of the momentum due to the recoil X-ray reflections is very important for the formation of PB with a definite wavelength. Therefore, one of the likely explanations is that the number of the atoms assessed by way of compensation for the recoil energy loss strongly depends on the temperature change of the crystal rigidity defined by $\Delta^{-1}(T)=N_{PCRRA}(T)$ (eq. (I-9) in App I) which is called as the partial charge rate of the recoil accommodation (PCRRA). Using this definition, eq. (3) is rewritten as follows (App I):

$$E_R(keV) = \frac{\Delta(T)}{2m}\cdot\frac{E_0^2}{c^2} \cong 5.37\cdot 10^{-10}\cdot\frac{E_0^2(keV)^2}{N_{PCRRA}(T)M_a(kg/mol)}, \tag{4}$$

in which $\Delta(T)$ ranges from zero for the rigid crystal at T=0 to one for the free atom at the melting point, i.e., $0 \le \Delta(T) \le 1$ ($\infty \ge N_{PCRRA}(T) \ge 1$). It naturally follows that $\Delta(T)$ might be deduced from the close theoretical relation of D-W factor. Although, in order to examine the characterization of PB, PCRRA as an unknown quantity should be theoretically derived from the first principles calculation, it is not purpose of this paper. PCRRA is treated here as a monotonic temperature dependent parameter without loss of generality. Therefore, eq. (4) based upon the above idea could be applied to not only the recoil-free nuclear γ-ray spectroscopy but also to recoil X-ray reflection over the energy region of 10 to 100keV. Here, it is assumed that the recoil velocity of the atom is sufficiently small so that it can be treated non-relativistically.

The accurately measured values of the dimension or mass of the crystal are indispensable for the determination of the atomic number of N in E_R. Hitherto, they have not been needed in the analysis of the experimental results of PB and ME. As a consequence, they have not been precisely recorded in almost all

reports. One of the experiments which is suitable for the present proposition is our observation of a new type of PB near Ga K edge of GaAs(200).[11-13] Some measured and calculated parameters are shown in Table II. In our experiment,[11-13] the flux of n=1.09·10^9 (*photons* / s 0.1% *band width*) in X-rays of nhv_0 was used at BL-6C$_1$ in the Photon Factory of KEK.[29]

III. The Bragg Law from the Accumulated Contraction of the Recoil Momentum of the Multi-reflex Photons based upon the Corpuscular Character of Light

An infinite crystal with discrete planes spaced with d_{hkl} along the z-axis is considered in Fig. 3. According to quantization by the old quantum theory, allowed motion of the crystal described by the momentum p_z along z-axis, which is constant in the absence of external forces working on the crystal, *i.e.*, $dp_z / dt = 0$, is given by

$$\oint p_z dz = p_z \int_0^{d_{hkl}} dz = p_z d_{hkl} = nh, \qquad (5)$$

where n is the quantum number relevant to the periodicity of d_{hkl} and h the Planck constant. Considering that $h = h/2\pi$ and $\boldsymbol{k}$ and $\boldsymbol{k}_0$ are the wave vector of the incident and reflected photons defined by $k = k_0 = 2\pi / \lambda_0$, and parallel to the recoil velocity of $\boldsymbol{v}$ and $\boldsymbol{v}_0$ defined by $v = v_0$ in eq. (I-8), respectively (Fig. 3), the z-component of the linear momentum p_z of the photon and crystal at the r-th time reflection in eq. (5) is given by

$$p_z = nh / d_{hkl} = \{(h/\lambda_0) - 2(r-1)\Delta(T)mv\}\sin\theta_B + \{(h/\lambda_0) - 2r\Delta(T)mv\}\sin\theta_B , \qquad (6a)$$

where r=1,2,⋯,l. Here, it should be noted that the Bragg law in eq. (6a) could not be derived as a natural result from $\Delta(T)$=1 at r=1 in the case of the free atom. By using the representation of the vector sum, the new Bragg law of eq. (6a) in Fig. 3 can be expressed by,

$$\boldsymbol{p} + \{\hbar \boldsymbol{k}_0 - 2(r-1)\Delta(T)m\boldsymbol{v}_0\} = \{\hbar \boldsymbol{k} - 2r\Delta(T)m\boldsymbol{v}\},$$

where p is the scattering vector. The scattering vector p is given by

$$\boldsymbol{p} = -\{\hbar \boldsymbol{k}_0 - 2(r-1)\Delta(T)m\boldsymbol{v}_0\} + \{\hbar \boldsymbol{k} - 2r\Delta(T)m\boldsymbol{v}\}. \qquad (6b)$$

Eq. (6a) is exactly identical with eq. (6b) and since $\boldsymbol{p}$ is a reciprocal vector, so is $-\boldsymbol{p}$.[30]

Paraphrasing eq. (6a) from the scheme of the Thomson scattering, [31] it follows that the first term of the incident photon with the momentum of $h/\lambda_0 - 2(r-1)\Delta(T)mv$ before absorption by an electron tightly bound to the atom in the crystal becomes $h/\lambda_0 - (2r-1)\Delta(T)mv$ as an excited state subjoined by $-\Delta(T)mv$ after absorption and it finally changes into $h/\lambda_0 - 2r\Delta(T)mv$ similarly subjoined again by $-\Delta(T)mv$ after emission. Similar to ME, there is a pair deficit of the recoil momentum of $2\Delta(T)mv$ by the crystal in eqs. (6a) and (6b) due to the absorption and emission in every reflection under the Bragg condition.

The momentum of the photon in the transmission via the absorption and emission under the non-Bragg condition of θ_B=0 in Fig 4 does not change without dissipation from D=1 in eq. (1). It is clear from the fact that maximum intensity of the forward scattering can be obtained from the maximum atomic form factor proportional to Z at the zero scattering angle. Moreover, since the recoil velocities of v_0 and v are parallel at the zero scattering angle and reverse sign each other in Fig 3, both recoil momentums offset instantaneously each other, i.e., v_0-v=0, because of zero intermediate state in the Thomson scattering.[31] This means that the transmission is the elastic scattering.

By using eq. (I-8) in App I, a new Bragg law from eqs. (6a) and (6b) is expressed as:

$$2d_{hkl}\sin\theta_B = \frac{n\lambda_0}{1-2r\Delta(T)\left(1-1/2r\right)} = n\lambda_0\{1+2r\Delta(T)\}, \qquad (7)$$

since $r>>1$ and $2r\Delta(T)<<1$ from Table III. By an approximation of $2r\Delta(T)\cong 0$ as the recoil-free reflection, the approximate Bragg law from eq. (7) is given by

$$2d_{hkl}\sin\theta_B = n\lambda_0.$$

It is important to stress that two types of PB from the transmitted and diffracted photons in Fig. 4 were derived on the basis of the new Bragg law in consideration of the multiple recoil reflections in eq. (7).

The term of $2r\Delta(T)$ in eq. (7) represents the relative change of the wavelength due to the momentum reduction by the r-time recoil reflections. After maximum reflections of l, the relative change of the wavelength is finally given by

$$\left(\frac{\Delta\lambda}{\lambda_0}\right)_R = l\left(\frac{\Delta\lambda}{\lambda_0}\right)_r = -l\left(\frac{\Delta\omega}{\omega_0}\right)_r = 2l\Delta(T) = 2l\frac{\delta(T)}{N}, \qquad (8)$$

where the multiplicity factor of the reflection for GaAs is given by (Fig. 3 and Table III)

$$l = \left[\frac{\mu}{d_{200}\cot\theta_B}\right]+1 = \left[\frac{2\cdot10^{-4}}{0.282\cdot10^{-9}\cdot\cot12.4^{\circ}}\right]+1 = 155{,}933, \qquad (9)$$

where [] is the Gauss' notation. The subscripts R and r in eq. (8) indicate the total and one time recoil reflection, respectively. It simply means that the frequency of X-rays changes by $\Delta\omega$ due to the recoil at every reflection, for example, as $\sin\omega_0 t$ to $\sin(\omega_0+\Delta\omega)t$ as shown in eq. (6a).

By using the bare beat formation formula of eq. (II-1) in App II, the variation in the intensity of a composite wave at the same spatial point at an instantaneous time, which is traditionally formed from *two distinct waves* with different frequencies $\omega_1=\omega_0$ and $\omega_2=\omega_0+\Delta\omega$ with the same amplitude A, could be expressed by

$$\psi(t) = A\sum_{i=1}^{2}\sin\omega_i t = A\sum_{r=0}^{1}\sin\left(\omega_0+r\Delta\omega\right)t$$

$$= \frac{A\sin\left(\omega_0+\Delta\omega/2\right)t\sin\Delta\omega t}{\sin\Delta\omega t/2} = 2A\sin\left(\omega_0+\Delta\omega/2\right)t\cos\Delta\omega t/2. \qquad (10)$$

If the sum of frequency as the average of $(\omega_1+\omega_2)/2(=\omega_0+\Delta\omega/2)$ was too high to be observed, eq. (10) would reduce to $\psi(t)\cong 2A'\cos[(\omega_1-\omega_2)t/2]=2A'\cos\Delta\omega t/2$, which is expressed by only the beat frequency as the beat pulsation.

Based upon the two wave approximation of DTXD, the long period of τ in eq. (10) is expressed by

$$\tau = 2\pi/[(\omega_1-\omega_2)/2] = 2/(\nu_1-\nu_2) = 2\lambda_1\lambda_2/c(\lambda_2-\lambda_1) = \lambda_{t_0}/c, \qquad (11)$$

where the wavelength of the beat λ_{t_0} is equal to twice the extinction distance t_0.[32] Eq. (11) is equivalent to $c\tau = 2t_0$ from the Kato-Lang's relation.[1] Therefore, by replacing $\lambda_1\cong\lambda_2$ and $\lambda_1-\lambda_2$ with λ_0 and $\Delta\lambda$, respectively, the relative change of the wavelength in eq. (11) from DTXD is represented by

$$\left(\Delta\lambda/\lambda_0\right)_{DTXD} = 2\lambda_0/\lambda_{t_0}, \qquad (12)$$

which should be equivalent to eq. (8), because both equations result from calalations based on understanding PB from different physical viewpoints.

By using the values of l and N for GaAs in Tables II and III, eq. (8) becomes

$$\left(\frac{\Delta\lambda}{\lambda_0}\right)_R \cong 2l\,\frac{\delta(300K)}{N} = \frac{2\times 155{,}933\cdot\delta(300K)}{8.91\cdot 10^{20}} = 3.50\cdot 10^{-16}\,\delta(300K)\,. \quad (13)$$

On the other hand, by using the values of λ_0 in Table II and λ_{t_0} for π -polarization of GaAs[33] in Table III, eq. (12) could be estimated to be

$$\left(\frac{\Delta\lambda}{\lambda_0}\right)_{DTXD} = \frac{2\lambda}{\lambda_{t_0}} = \frac{2\times 0.1207\cdot 10^{-9}}{110.08\cdot 10^{-6}} \cong 2.19\times 10^{-6}. \quad (14)$$

The values of δ (300K) and Δ(300K) can then be obtained from the equivalence of eqs. (13) and (14) as in Table III. The reciprocal of Δ(300K) gives N_{PCRRA}(300K) =1.42 · 10^{11} in eq. (4) which is the effective number of the atoms in the crystal compensating the recoil energy as PCRRA and δ^{-1}(300K) = 1.60 · 10^{-10} represents a ratio of N_{PCRRA}(300K)/N. A value of the wavelength difference of $\Delta\lambda$ from eq. (14) is estimated to be 0.264fm. By using M_a = 0.069723kg/mol for Ga, the recoil energy loss $2E_R$ per Ga atom by a single photon for formation of PB in eq. (4) is estimated to be

$$2E_R(keV) \cong \frac{5.37\cdot 10^{-10}\times 10.268^2(keV)^2}{1.42\cdot 10^{11}\times 0.069732(kg/mol)} \cong 11.41\cdot 10^{-18}(keV)\,.$$

These physical quantities related with PB of GaAs near Ga K edge in Table III are commonly too infinitesimal to be detected directly by means of the active detectors, because their detection ability is clearly outside the range of their sensitivity. They could be barely obtained from PB through the interference of the multiple photons.

IV. Formation of PB and its Characterization

IVA. The Effect of the binomial distribution on the quasi-collimation of the definite translational state photons.

Fig. 4 schematically shows the formation of the diffracted and transmitted photons. All of the diffracted components of a photon are reflected by odd multiples and their wave vectors make the angle of 2θ_B with the incident photon. The transmitted components of a photon are reflected by even multiples and are parallel to the incident photon. Generally there are two ways in Figs 5(a) and 5(b) to count the numbers of the photon paths from combinations of the diffraction (d) and transmission (t) as stochastic events by the binomial distribution (BD) in Fig. 4.

Fig 5(a) shows one way to count the photon paths by d and t in Fig 4, which are designated as G-wave (G) and O-wave (O) in the two wave approximation in DTXD, respectively. In Fig 5(a), when an incident photon is injected to the net plane d_{hkl} from the upper left or right of the test crystal under the Bragg condition setting, it splits into G and O in each case. The former makes an angle of 2θ_B with the incident photon and the latter parallel to it. In this scheme, the alternatives are G and O as described by G=O =1/2 (G+O=1) and then all of paths in the multiplicity l could be given by BD of $B(G,\ l)=(G+O)^l$=1. However, the path in Fig 5(a) discriminates against only the *direction* between G and O by arrows determined from the incident photon, without discrimination between the Bragg reflection and transmission. As a result, the number of the diffraction

in Fig 4 can not be determined by the path of Fig 5(a) and it is impossible to classify the emitted photons into two groups of the transmitted and diffracted photons as shown.

In other path in Fig 5(b), it is not important whether the angle between the incident and reflected photons correlates as in the former case but whether the photon diffracts (d) or advances (t) in a beeline at each reflection point. In this case, the number of the diffraction is countable from number of flexion (d) and beeline (t) in each path in Fig 5(b), for example, one diffraction from $d \cdot t$ of the diffraction-transmission or $d \cdot t$ of the transmission-diffraction and double diffraction from the diffraction-diffraction of $d \cdot d$ and no diffraction from the transmission-transmission of $t \cdot t$ in the case of l=2. Similarly the alternatives are Bragg reflection (d) and transmission (t) of fifty-fifty in spite of two kinds of the incident photon and there is a sharp distinction between them. In the section IVC, the construction of the intrinsic beat functions modulated by BD from the bare beat formation formulas in eqs. (II-1) and (II-2) in App II using the way of Fig 5(b) will be shown. It is important that one-to-one correspondence between the two ways of Figs 5(a) and 5(b) to count the optical paths in Fig 4 is clearly satisfied from $B(G, l)=B(d, l)=1$.

On the assumption that the statistical probability of d and t is $d=t=1/2$ under $d+t=1$, the numbers of the photon paths from the combination of d and t by BD in Fig 5(b) could be counted by

$$B(l, d) = (d+t)^l = \sum_{r=0}^{l} {}_lC_r d^{l-r} t^r = (1/2)^l \sum_{r=0}^{l} {}_lC_r = 1. \qquad (15)$$

Using three-dimensionally arrayed net planes (hkl) as reflectors in a crystal constructed by atoms with the definite interval by d_{hkl} in the directions of [hkl], after an incident single photon is reflected in even and odd times, its components are emitted as the transmitted and diffracted photons of l modes in each in case of multiplicity factor l in Fig. 4, respectively. Both of the diffracted and transmitted photons produce PB by the principle of the superposition of both components, which are the definite *translational states* with information about the location and momentums.[34]

According to Dirac,[34] the photon is described as going partly into each of the two components into which the incident beam is split. The photon is then in a translational state given by the superposition of the two translational states associated with the two components. For a photon to be in a definite translational state it need not be associated with one single beam of X-ray, but may be associated with two or more beams of X-ray which are the components into which one original beam has been split. In the accurate mathematical theory, each translational state is associated with one of the wave function of ordinary wave optics which describe either a single beam or two or more beams into which one original beam has been split. Translational states are thus superposable in a similar way to wave functions.

The midline in the Pascal's triangle (PT) of the binomial coefficients in eq. (15) (Table IV), which geometrically depict the Borrmann fan in Fig. 4 is an axis of bilateral symmetry from the relation ${}_lC_r = {}_lC_{l-r}$. PT in eq. (15) is constructed from the Pascal's formula of ${}_lC_r = {}_{l-1}C_{r-1} + {}_{l-1}C_r$. By using the formulas and the Stirling's approximation of $l! = \sqrt{2\pi}\, l(l/e)^l$, the peak values of the probability functions in BD in the pair of the odd and even integers ($2l_h+1$, $2l_h+2$) of l, are mutually identical and shown in Table IV as

$$B(2l_h+2,d)\big|_{r=l_h+1}=(1/2)^{2l_h+2}\cdot_{2l_h+2}C_{l_h+1}=(1/2)^{2l_h+1}\cdot_{2l_h+1}C_{l_h+1}=B(2l_h+1,d)\big|_{r=l_h+1}\cong\frac{1}{\sqrt{\pi l_h}}.$$

This is estimated to be $2.02\cdot10^{-3}(>>1/l_h)$ per one photon for $l=2l_h+1=155{,}933$ of GaAs in Table III. In the case of the photon flux $n = 1.09\cdot10^9$ (photons/s 0.1% band width) in KEK[29], the peak intensity is given by the rate $2.20\cdot10^6$ (photons·0.1% band width). It is understood from the fact that the shape of $B(l,d)$ for large l is approximated as the normal distribution, B (e, d) that closely resembles a hanging bell with the inflection.

Similarly, the values of the probability functions for d^l and $d^{l-1}t$ along the midline and t^l and dt^{l-1} along the right and left sides of the Borrmann fan for GaAs are given by

$$B(l,d)\big|_{r=0orl}=(1/2)^l\cdot_l C_0=(1/2)^l\cdot_l C_l=1/2^l=1/2^{155,933}\cong0,$$

for d^l and t^l, and

$$(1/l)B(l,d)\big|_{r=l-1orl}=(1/2)^l(1/l)_l C_1=(1/2)^l=1/2^{155,933}\cong0,$$

for dt^{l-1} and $d^{l-1}t$, which are only one among l terms of the l degree of $t\cdot t\cdots d\cdots t\cdot t$ and $d\cdot d\cdots t\cdots d\cdot d$, respectively (See Fig 4 in the case of l =5). These are used for the steep contraction of the projecting peaks stated later in the section IVC.

It follows that, although the incident photon seems to apparently diverge with an angle of $2\theta_B$ at the pivot of the fan in Fig 4, the reflected photons of the higher order of r in the approximated product near $(dt)^r$ ($r\approx n/2$) are highly probable given by the large binomial coefficients in the vicinity of the midline in PT as if the photons are apparently collimated. It turns out that the multi-reflex photons can be considered to be quasi-collimated to 68.3% within ± 198 ($=\sqrt{ldt}$) modes as the standard deviation from the normal distribution approximated from eq. (15). Experimentally, when the crystal is set at the Bragg law, so that the transmitted and diffracted photons exist, the point of emergence can be determined by taking several film recordings at different distances from the crystal. In doing this, it is found that the point of emergence for the transmitted and diffracted photons is directly opposite the entrance point, suggesting that the effective combination of the two beams has traveled through the crystal parallel to the diffracting planes. This has been called as the Borrmann effect.[35-37] The Borrmann effect can therefore be understood as the quasi-collimation from AM effect of BD.

IVB. The formation of bare PB due to the transmitted and diffracted photons more than two by multiple reflections

Taking account of the probability distribution of BD in eq. (15) as a statistical weight of the reflected photons by the three-dimensionally arrayed reflectors, the intrinsic PB can be detemined from the superposition of the expected values of the even and odd time multi-reflex photons. From the addition and subtraction between weighted forms of eqs. (II-1) and (II-2) in App II with BD, it is deduced that

$$\psi_{\substack{trans\\diff}}(t)=\frac{A}{2}\left\{(\psi_{trans}+\psi_{diff})\pm(\psi_{trans}-\psi_{diff})\right\}$$
$$=\frac{A}{2}\left\{\left(\frac{1}{2}\right)^l\sum_{r=0}^{l}\binom{l}{r}\sin(\omega_0+r\Delta\omega)t\pm\left(\frac{1}{2}\right)^l\sum_{r=0}^{l}(-1)^r\binom{l}{r}\sin(\omega_0+r\Delta\omega)t\right\},\qquad(16)$$

where the subscripts of *trans* and *diff* are abbreviated from *transmission* and *diffraction*, the double subscripts

of $\begin{cases} trans \\ diff \end{cases}$ match with $\pm$ in ψ and $\begin{pmatrix} l \\ r \end{pmatrix}$ is equivalent to ${}_lC_r$.

In order to characterize the nature of two types of PB by $\psi_{\substack{trans \\ diff}}$, it is important to characterize the bare beats of $\psi_{\pm}(t)$ without BD. The bare beat of $\psi_{+}(t)$ due to the transmitted photons given by the sum of eqs. (II-2) and (II-1) is represented by

$$\psi_{+}(t) = \frac{A}{2}\left\{\frac{\sin\left[\omega_0 + \frac{l}{2}\Delta\omega\right]t \cdot \sin\frac{l+1}{2}\Delta\omega t}{\sin\frac{\Delta\omega t}{2}} + \frac{\sin\left[\omega_0 t + \frac{l}{2}(\Delta\omega t + \pi)\right] \cdot \sin\frac{l+1}{2}(\Delta\omega t + \pi)}{\cos\frac{\Delta\omega t}{2}}\right\}$$

$$= \begin{cases} \dfrac{A\sin[\omega_0 + (l-1)\Delta\omega/2]t \cdot \sin(l+1)\Delta\omega t/2}{\sin\Delta\omega t} & l: odd \qquad (17) \\ \dfrac{A\sin(\omega_0 + l\Delta\omega/2)t \cdot \sin(l+2)\Delta\omega t/2}{\sin\Delta\omega t} & l: even. \qquad (18) \end{cases}$$

Similarly, $\psi_{-}(t)$ from the subtraction between them is given by

$$\psi_{-}(t) = \frac{A}{2}\left\{\frac{\sin\left[\omega_o + \frac{l}{2}\Delta\omega\right]t \cdot \sin\frac{l+1}{2}\Delta\omega t}{\sin\frac{\Delta\omega t}{2}} - \frac{\sin\left[\omega_o t + \frac{l}{2}(\Delta\omega t + \pi)\right] \cdot \sin\frac{l+1}{2}(\Delta\omega t + \pi)}{\cos\frac{\Delta\omega t}{2}}\right\}$$

$$= \begin{cases} \dfrac{A\sin[\omega_0 + (l+1)\Delta\omega/2]t \cdot \sin(l+1)\Delta\omega t/2}{\sin\Delta\omega t} & l: odd \qquad (19) \\ \dfrac{A\sin(\omega_0 + l\Delta\omega/2)t \cdot \sin l\Delta\omega t/2}{\sin\Delta\omega t} & l: even. \qquad (20) \end{cases}$$

All of the coefficients of $\Delta\omega t$ in the second sine function in the numerators of eqs. (17), (18), (19) and (20) are even integer. By replacing l by odd integer $2l_h$+1 or by even one $2l_h$ these equations can be simplified. It should be noted that these four equations with large l are identical with the basic generating function of the bare beat formation formula in eq. (II-1) in App II.

In case of GaAs (200) with odd integer of l=$2l_h$+1=155,933 in eq. (9) (Table III), eqs. (17) and (19) can be simply rewritten in the general forms as follows:

$$\psi_{\pm}^{l=2l_h+1}(t) = \begin{cases} \dfrac{A\sin(\omega_0 + l_h\Delta\omega)t\sin(l_h+1)\Delta\omega t}{\sin\Delta\omega t} & transmission(+) \\ \dfrac{A\sin[\omega_0 + (l_h+1)\Delta\omega]t\sin(l_h+1)\Delta\omega t}{\sin\Delta\omega t} & diffraction(-) \end{cases} \qquad (21a)$$

In the case of even integer of l=$2l_h$, eqs. (18) and (20) can be rewritten as follows:

$$\psi_{\pm}^{l=2l_h}(t) = \begin{cases} \dfrac{A\sin(\omega_0 + l_h\Delta\omega)t\sin(l_h+1)\Delta\omega t}{\sin\Delta\omega t} & transmission(+) \\ \dfrac{A\sin(\omega_0 + l_h\Delta\omega)t\sin l_h\Delta\omega t}{\sin\Delta\omega t} & diffraction(-) \end{cases} \qquad (21b)$$

It should be noted here that $\psi_{-}^{l=2lh}(t)$ is expressed in term of sin $l_h\Delta\omega t$ in the second sine function in the numerator, which differ from others because of difference in value between even integers l=$2l_h$ and odd integers

l=2l_h+1.

Since ω_0 is much higher than $l_h\Delta\omega$ and $(l_h+1)\Delta\omega$ in Tables II and III and the sum frequency is too high to be observed, by using eq. (III-6) in App III and replacing $A\sin(\omega_0+l_k\Delta\omega)t$ and $A\sin[\omega_0+(l_k+1)\Delta\omega]$t with A', a set of eq. (21a) and $\psi_+^{l=2l_h}(t)$, and independently $\psi_-^{l=2l_h}(t)$ in eq. (21b) reduce to the direct product of the regular form as

$$\psi_{\pm}^{l=2l_h+1}(t)\cong\psi_{+}^{l=2l_h}(t)\cong 2^{l_h}A'\prod_{r=1}^{l_h}\sin\left(\Delta\omega t+r\pi/(l_h+1)\right), \tag{22a}$$

and

$$\psi_{-}^{l=2l_h}(t)\cong 2^{l_h-1}A'\prod_{r=1}^{l_h-1}\sin\left(\Delta\omega t+r\pi/l_h\right), \tag{22b}$$

where the beat frequencies of $l_h\Delta\omega$ and $(l_h-1)\Delta\omega$ appear in eqs. (22a) and (22b), respectively.

The probability density at r in (15) is positive definite as $0<(1/2)^l{}_lC_r<1$. As a result, the absolute values of the cross products in eq. (16) between $\psi_\pm(t)$ and $B(l,d)$ shrink systematically and inhomogeneously and they satisfy the inequality

$$\begin{aligned}\left|\psi_{\substack{trans\\diff}}(t)\right| &= \left|\frac{A}{2}\left(\frac{1}{2}\right)^l\sum_{r=0}^{l}\left[\binom{l}{r}\sin(\omega_0+r\Delta\omega)t\pm(-1)^r\binom{l}{r}\sin(\omega_0+r\Delta\omega)t\right]\right| \\ &< \left(\frac{1}{2}\right)^l\sum_{r=0}^{l}\binom{l}{r}\cdot\left|\frac{A}{2}\left[\sin(\omega_0+r\Delta\omega)t\pm(-1)^r\sin(\omega_0+r\Delta\omega)t\right]\right| \\ &\le \left|\frac{A}{2}\sum_{r=0}^{l}\left[\sin(\omega_0+r\Delta\omega)t\pm(-1)^l\sin(\omega_0+r\Delta\omega)t\right]\right| = \left|\psi_\pm(t)\right|\le\left|\cos\mathrm{ec}\Delta\mathrm{w}t\right|. \end{aligned} \tag{23}$$

For brevity, Figs. 6(a) l_h=1, (b) l_h=2, (c) l_h=3, (d) l_h=4, (e) l_h=19, (f) l_h=20, (g) l_h=29 and (h) l_h=30 show the modulated *cosine* curves for the small odd and even integers of l_h instead of l_h=77966 in eq. (22a). Here it should be noted that the behavior of all curves in Fig 6 as well as Fig 7 is graphed by eqs. (22a) and (22b). All of the curves have the alternating and non-alternating projecting peaks at every π -radian depending on the even and odd integers of l_h in eqs. (22a) and (22b), respectively. The height of all peaks in eqs. (22a) and (22b) by using eq. (III-6) are characterized as

$$\begin{aligned}\underset{\Delta\omega t\to m\pi}{Lim}\frac{\sin(l_h+1)\Delta\omega t}{\sin\Delta\omega t} &= \underset{\delta\to 0}{Lim}\frac{\sin(l_h+1)(m\pi+\delta)}{\sin(m\pi+\delta)}\left\{=2^{l_h}\prod_{r=1}^{l_h}(-1)^m\sin\frac{r}{l_h+1}\pi\right\} \\ &= (-1)^{ml_h}(l_h+1)=\begin{cases}l_h+1 & (l_h:even)\\ -(l_h+1) & (l_h,m:odd)\end{cases}.\end{aligned} \tag{24a}$$

and

$$\begin{aligned}\underset{\Delta\omega t\to m\pi}{Lim}\frac{\sin l_h\Delta\omega t}{\sin\Delta\omega t} &= \underset{\delta\to 0}{Lim}\frac{\sin l_h(m\pi+\delta)}{\sin(m\pi+\delta)}\left(=2^{l_h-1}\prod_{r=1}^{l_h-1}(-1)^m\sin\frac{r}{l_h}\pi\right) \\ &= (-1)^{m(l_h-1)}l_h=\begin{cases}l_h & (l_h:odd)\\ -l_h & (l_h:even,m:odd).\end{cases}\end{aligned} \tag{24b}$$

All of the curves in Fig. 6 show the behavior of $\sin(l_h+1)\Delta\omega t$ $\mathrm{cosec}\,\Delta\omega t$ due to AM and FM that is observed only in the half wave of the projecting peaks (Fig. 7).

In order to investigate AM and FM effects by $\mathrm{cosec}\,\Delta\omega t$ in eqs. (22a) and (22b) in detail, the modulated

cosine curves of $\sin(l_h+1)\Delta\omega t \operatorname{cosec}\Delta\omega t$ together with the non-modulated curves of $\sin(l_h+1)\Delta\omega t$ for case of l_h=9 and 10, respectively, are shown in Figs. 7(a) and (b). For example, in Fig. 7(a) over an angular ranges of $|\Delta\omega t| \leq 18^\circ$, $162^\circ \leq \Delta\omega t \leq 198^\circ$ and $342^\circ \leq \Delta\omega t \leq 378^\circ$, the projecting peak of l_h+1=10 in the height of the half-wave due to AM are seen, together with FM of the half frequency of $(1/2)\Delta\omega$ as understood from the anti-phase region between two peaks at 180° and 360°. FM could not be seen in range of $18^\circ \leq \Delta\omega t \leq 162^\circ$ and $198^\circ \leq \Delta\omega t \leq 342^\circ$, but AM of the amplitude of the projecting peak can be seen in all of the curves in Figs.6 and 7, except Fig. 6 (a).

Fig. 6(a) in eq. (10) is a simple *cosine* curve constructed by the continuation of only the projecting peaks with the amplitude of 2 (=l_h+1), as a special treatment without damped waves seen in others. Eq. (10) is conventionally applicable to, for example, the first observed beats of the sound waves, such as those produced by two tuning forks with different frequencies, which is in long waves with low directivity without rigid limitation such as given by the Bragg law. Optical beat was first observed by Forrester et al.[38] In order to obtain two waves of slightly different frequency, which is important to distinguish the waves, they use the energy level splitting of Hg atoms of a discharge lamp due to the Zeeman effect was used. The emitted light contains two components of frequencies ν_1 and ν_2 which differ in proportion to the applied magnetic field. When these components are recombined at the surface of a photoelectric mixing tube, the beat frequency ν_1-ν_2 is generated. The photoelectric current was proportional to $\psi^2(t)$.[38]

IVC. The AM effect of the binomial distribution on bare PB and its projecting peaks

IVC-i. Analysis of intrinsic PB by BD.

The number of different paths, counted based upon ${}_lC_r d^{l-r} t^r$ (r=1,2,・・・,l) by way of Fig 5(b), is derived from the degree of d and t according to their permutation in Fig. 4. In the case of a mono-layer crystal of l=1 in Fig. 8(a), an incident photon splits into the two components by $(d+t)^1 = d+t$ of BD in eq. (15) as follows:

[1] The diffracted photon d 1 diffraction (no. of d: odd)

[2] The transmitted photon t 0 diffraction (no. of d: even).

Considering BD of $(d+t)^1={}_1C_0 d+{}_1C_1 t=(1/2)\{[1]+[2]\}$ from PT (Table IV), both of the diffracted and transmitted photons in eq. (16) are given by

$$\psi_{diff}^{l=1}(t) = (A/2)\sin(\omega_0+\Delta\omega)t \quad \text{and} \quad \psi_{trans}^{l=1}(t) = (A/2)\sin\omega_0 t,$$

respectively. The bare diffracted and transmitted photons without BD are expressed by

$$\psi_{-}^{l=1}(t) = A\sin(\omega_0+\Delta\omega)t \quad \text{and} \quad \psi_{+}^{l=1}(t) = A\sin\omega_0 t$$

in eqs. (19) and (17), respectively. The AM effect of BD on them is found to be half of the amplitude. It is clear that they could not form PB but only the Bragg spot, since there is only one photon in each diffraction and transmission in Fig 8(a).

In the case of l=2 in Fig. 8(b), the spacing in the double layer crystal is equal to $d_{hkl}\cot\theta_B$ in eq. (9) and the multiplicity l=2. Here, the order of the letters d and t in Figs 8(b) represent the reflection process due to the elapsed time. Then, for example, $d \cdot t$ is not equivalent to $t \cdot d$ as a process stated in the section IVA. Emitted

photons from $(d+t)^2 = d\cdot t+t\cdot d+d\cdot d+t\cdot t$ of BD in eq. (15) are represented as follows:

[1] Diffracted photon $d\cdot t$ 1 diffraction (no. of d: odd)

[2] Diffracted photon $t\cdot d$ 1 diffraction (no. of d: odd)

[3] Transmitted photon $d\cdot d$ 2 diffraction (no. of d: even)

[4] Transmitted photon $t\cdot t$ 0 diffraction (no. of d: even).

In Fig 8(b), the diffracted photons from $d\cdot t$ and $t\cdot d$ successively at the 1st and 2nd layer in order are together expressed by eq. (16) as follows:

$$\psi_{diff}^{l=2}(t) = (A/2)\sin(\omega_0 + \Delta\omega)t,$$

Therefore, the diffracted photons from $d\cdot t$ and $t\cdot d$ could not form PB, since there is no difference in the frequencies to form a beat between [1] and [2]. Intrinsic PB formed by the superposition of the transmitted photons of [3] and [4] by $d\cdot d$ and $t\cdot t$ at the 1st and 2nd layer are given by eq. (16) as follows:

$$\psi_{trans}^{l=2}(t) = (A/2)\sin(\omega_0 + \Delta\omega)t\cos\Delta\omega t. \qquad (|\psi_{trans}^{l=2}(t)| \le A/2)$$

While the bare diffracted photons and bare transmitted PB are given by

$$\psi_{-}^{l=2}(t) = A\sin(\omega_0 + \Delta\omega)t \quad \text{and} \quad \psi_{+}^{l=2}(t) = 2A\sin(\omega_0 + \Delta w)t\cos\Delta\omega t$$

by eqs. (20) and (18), respectively. The AM effect of BD is found to be half of the amplitude. As a whole, the sum of [1]+([2]+[3])+[4]=$d\cdot t$+($t\cdot d$+$d\cdot d$)+$t\cdot t$ in Fig 8(b) becomes BD of $(1/2)^2\sum_{r=0}^{2} {}_2C_r$ = $(1/2)^2$ (1+2+1), which satisfy PT (Table IV).

In the case of l=3 in Fig. 8(c), the six kinds of the emitted photons from $(d+t)^3$ of the triple layer crystal by BD in eq. (15) are described as follows:

[1] Diffracted photon $d\cdot t\cdot t$ 1 diffraction (no. of d: odd)

[2] Diffracted photon $d\cdot d\cdot d + t\cdot d\cdot t$ 3 and 1 diffraction (no. of d: odd)

[3] Diffracted photon $t\cdot t\cdot d$ 1 diffraction (no. of d: odd)

[4] Transmitted photon $d\cdot t\cdot d$ 2 diffraction (no. of d: even)

[5] Transmitted photon $d\cdot d\cdot t + t\cdot d\cdot d$ 2 diffraction (no. of d: even)

[6] Transmitted photon $t\cdot t\cdot t$ 0 diffraction (no. of d: even).

In eq. (16), both intrinsic PB of the diffracted and transmitted photons are given by

$$\psi_{diff}^{l=3}(t) = (3A/8)\sin(\omega_0 + \Delta\omega)t + (A/8)\sin(\omega_0 + 3\Delta\omega)t \qquad (|\psi_{diff}^{l=3}(t)| \le A/2)$$

and

$$\psi_{trans}^{l=3}(t) = (A/8)\sin\omega_0 t + (3A/8)\sin(\omega_0 + 2\Delta\omega)t, \qquad (|\psi_{trans}^{l=3}(t)| \le A/2)$$

respectively. Both bare PB without BD are given by

$$\psi_{-}^{l=3}(t) = 2A\sin(\omega_0 + 2\Delta\omega)t\cos\Delta\omega t$$

by eq.(19), and

$$\psi_{+}^{l=3}(t) = 2A\sin(\omega_0 + \Delta\omega)t\cos\Delta\omega t$$

by eq. (17). The AM effect of BD could be found in the sum of the coefficients A/2 in $\psi_{diff}^{l=3}(t)$ and $\psi_{trans}^{l=3}(t)$, which are a quarter of 2A in $\psi_{\pm}^{l=3}(t)$. In Fig 8(c), [1]+([2]+[4])+ ([3]+[5])+[6]=$d\cdot t\cdot t$ + ($d\cdot d\cdot d + t\cdot d\cdot t + d\cdot t\cdot d$) + ($t\cdot t\cdot d + d\cdot d\cdot t + t\cdot d\cdot d$) + $t\cdot t\cdot t$ similarly satisfies PT in BD of $(1/2)^3\sum_{r=0}^{3} {}_3C_r$= $(1/2)^3$ (1+3+3+1) (Table IV).

To characterize a new PB from the superposition of three waves, in a manner similar to the case of l=4 without the distribution diagram of optical path, the eight photons from $(d+t)^4$ of BD in eq. (15) in the quadruple layer crystal are as follows:

[1] Diffracted photon $d\cdot t\cdot t\cdot t$ 1 diffraction (no. of d: odd)

[2] Diffracted photon $d\cdot t\cdot d\cdot d + d\cdot d\cdot d\cdot t + t\cdot d\cdot t\cdot t$ 3 and 1 diffraction (no. of d: odd)

[3] Diffracted photon $d\cdot d\cdot t\cdot d + t\cdot d\cdot d\cdot d + t\cdot t\cdot d\cdot t$ 3 and 1 diffraction (no. of d: odd)

[4] Diffracted photon $t\cdot t\cdot t\cdot d$ 1 diffraction (no. of d: odd)

[5] Transmitted photon $d\cdot t\cdot t\cdot d$ 2 diffraction (no. of d: even)

[6] Transmitted photon $d\cdot t\cdot d\cdot t + d\cdot d\cdot d\cdot d + t\cdot d\cdot t\cdot d$ 4 & 2 diffraction (no. of d: even)

[7] Transmitted photon $d\cdot d\cdot t\cdot t + t\cdot d\cdot d\cdot t + t\cdot t\cdot d\cdot d$ 2 diffraction (no. of d: even)

[8] Transmitted photon $t\cdot t\cdot t\cdot t$ 0 diffraction (no. of d: even).

Both intrinsic PB of the diffracted and transmitted photons in eq. (16) are represented as follows:

$$\psi_{diff}^{l=4}(t) = (A/4)\{\sin(\omega_0 + \Delta\omega)t + \sin(\omega_0 + 3\Delta\omega)t\}$$
$$= (A/2)\sin(\omega_0 + 2\Delta\omega)t\cos\Delta\omega t \qquad (|\psi_{diff}^{l=4}(t)| \le A/2)$$

and

$$\psi_{trans}^{l=4}(t) = (A/16)\sin\omega_0 t + (6A/16)\sin(\omega_0 + 2\Delta\omega)t$$
$$+(A/16)\sin(\omega_0 + 4\Delta\omega)t, \qquad (|\psi_{trans}^{l=4}(t)| \le A/2)$$

which is constructed by three waves with different amplitudes and frequencies as the first new PB. The bare PB of the diffracted and transmitted photons is represented by

$$\psi_{-}^{l=4}(t) = 2A\sin(\omega_0 + 2\Delta\omega)t\cos\Delta\omega t$$

by eq. (20) and

$$\psi_{+}^{l=4}(t) = A\frac{\sin(\omega_0 + 2\Delta\omega)t\cdot\sin 3\Delta\omega t}{\sin\Delta\omega t}$$
$$= 4A\sin(\omega_0 + 2\Delta\omega)t\cdot\sin(\Delta\omega t + \pi/3)\cdot\sin(\Delta\omega t + 2\pi/3),$$

by eqs. (18) and (III-6) in App III. Considering $\psi_{+}^{l=4}(t) \le 3$ as shown in Fig 6(b), it is apparent that the sum of the coefficients A/2 in $\psi_{\substack{trans\\diff}}^{l=4}(t)$ baries from a quarter of 2A in $\psi_{-}^{l=4}(t)$ to a sixth of 3A in $\psi_{+}^{l=4}(t)$. From the above distribution of optical paths, PT is confirmed by [1]+{[2]+[5]}+{[3]+[6]}+{[4]+[7]}+[8]=

$(1/2)^4\sum_{r=0}^{4} {}_4C_r = (1/2)^4(1+4+6+4+1)$ (Table IV).

IVC-ii. Remarks on the AM effect of BD on PB, including the projecting peaks.

Figs 9(b), (c), (e) and (f) show four curves of intrinsic PB of $\psi_{trans}^{l=3}(t)$, $\psi_{diff}^{l=3}(t)$, $\psi_{trans}^{l=4}(t)$ as a new beat and $\psi_{diff}^{l=4}(t)$, respectively. It should be noted that all of these curves show the very clean and accurate interference fringes consisting of periodical pairs of a maximum and a minimum or *belly* and *node* as the transmitted and diffracted PB as discussed in ref. 38. It is evident in eq. (22b) that the height of the projecting peak and the beat wave number of $\psi_{-}^{l=4}(t)$ could be determined from l_h=2. Therefore, both bare PB of $\psi_{-}^{l=3}(t)$ and $\psi_{-}^{l=4}(t)$ are perfectly identical from the sum frequency of $\omega_0 + 2\Delta\omega$. However, the intrinsic PB of both

$\psi_{diff}^{l=3}(t)$ and $\psi_{diff}^{l=4}(t)$ in Fig 9(c) and (f), respectively, is modulated in amplitude due to the cross product between $\psi_{-}^{l=3\&4}(t)$ and BD. Similarly, from the sum frequency characteristic $\omega_0 + \Delta\omega$, Fig 10(a) displays the curve of bare PB of $\psi_{+}^{l=3}(t)$, which should fit the curve of intrinsic PB $\psi_{trans}^{l=3}(t)$ modulated by BD in Fig 9(b). Curve of Fig 9(e) is the new intrinsic PB from three different photons described by $\psi_{trans}^{l=4}(t)$. Fig 10(b) shows the curve of bare PB of $\psi_{+}^{l=4}(t)$, whose envelope in eq. (22a) is shown in Fig 6(b). The remarkable variations influenced by both the projecting and damped peaks in Fig 10(b) could not be perfectly found in Fig 9(e) and reformed to the typical interference fringe by AM effects by BD.

All of the prominently projecting peaks shown in Fig 6 emerge at $m\pi$ (m=1,2,$\cdots$) in eqs. (24a) and (24b), which coincide with the base angles and the midline in PT in Fig 4. They are remarkably contracted by BD in Fig 9 in the case of l=3 and 4 as well as l=2. Generally, according to the AM effect of BD indicated in the section IVA, the expected values of the relevant projecting peaks with the height $\pm(l_h + 1)$ and $\pm l_h$ in eqs. (24a) and (24b), respectively, could be contracted as follows:

$$\left.\begin{array}{lll} d^l & & \pm(l+1)B(l,d)\big|_{r=0 or l} \\ \overline{dt^{l-1}} & \text{or} & \\ & t^l & \\ & d^{l-1}t & (\pm(l+1)/l)B(l,d)\big|_{r=l-1 or 1} \end{array}\right\} = \pm\frac{l+1}{2^l}$$

$$\cong \pm\left(\frac{\sqrt[l]{l}}{2}\right)^l \cong \pm\frac{1}{2^l} = \pm\frac{1}{2^{155,933}} \cong 0.^{39}\ (l>>1).$$

For example, the peak values of $\pm(l+1)/2^l$ are estimated to be $\pm$ 1 for l=1, $\pm$ 3/4 for l=2, $\pm$ 1/2 for l=3, $\pm$ 5/16 for l=4,$\cdots$, $\pm$ 155,934/$2^{155,933}$ for l=155,933, which decrease steeply with increasing l. All of these values are rapidly contracted as if erased by AM effect of BD in Fig 9.

From the considerations of the multiple reflections in the crystals from 1 to 4 of l in the preceding section, $\left|\psi_{\substack{trans\\diff}}(t)\right| < \left|\psi_{\pm}(t)\right|$ in eq. (23) is generally satisfied due to AM effect of BD. Especially, there is clear evidence in support of eq. (23) in all intrinsic PB, in which amplitudes of $\psi_{\substack{trans\\diff}}(t)$ are contracted from a quarter of the amplitudes of two wave bare PB to a sixth of those of three wave bare PB.

It is clear from the superimposed graphs of $\psi_{trans}^{l=3}(t)$ and $\psi_{diff}^{l=3}(t)$ in Fig 9(d) that the periods of both PB are to be 2π sec. as seen in the envelope of "cos t" in eq. (22a) (Fig 6(a)). In the graphs of $\psi_{trans}^{l=4}(t)$ and $\psi_{diff}^{l=4}(t)$ in Fig 9(g), they have the appearance of a coincidence between their periods, in opposition to the fact. The period of $\psi_{trans}^{l=4}(t)$ is determined to be π sec. by $f(0) = f(\pi) = 3$ from the envelope as $f(t) = 4\sin(-t + \pi/3)\cdot\sin(-t + 2\pi/3)$ defined by eq. (22a) (Figs 6(b) and 10(b)). In spite of the difference of the period, the superimposition of $\psi_{trans}^{l=4}(t)$ on $\psi_{diff}^{l=4}(t)$ in Fig 9(g) is reasonably understood.

In $l \geq 5$, the pair appearance of PB by the transmitted and diffracted photons with more than two photons could be similarly confirmed one by one in each term of $(d+t)^l$, together with the validity of eq. (23), including the disappearance of all the projecting peaks by AM effect of BD. It is important to stress that eqs. (17), (18), (19) and (20) are reasonable as the bare beat formation formulas of PB. It allows me to frame a new definition of the beat that is both comprehensive and accurate.

Although analytical forms of eq. (16) could not be obtained in the present work, it is important to understand the results of PB caused by the multiple recoil reflections received double AM from both cosec $\Delta\omega t$ and $B(l,d)$.

The expected profiles of PB in eq. (16) might be considerably deformed due to the following factors: (i) low photon counting rate of the detectors, (ii) slow A-D converters, (iii) overflow or miscount of the photons (iv) local damages, unevenness or corrugation in both surfaces of the crystal and their parallelism, (v) unsuitable time-constant for the measuring instrument system, (vi) convolution of the response and resolution function of the instruments, etc. It is apparent that the factors cause either broadening or narrowing of the PB profile in each. For example, an uncertainty in the thickness of our GaAs crystal is estimated to be $\Delta\mu / \mu \cong 0.03$ as determined from non-parallellsm and roughness of the surfaces. From eq. (22a), two types of the transmitted and diffracted PB comprise both *eq*.(17)/*eq*.(18) and *eq*.(19)/*eq*.(20) hybrids from the uncertainty of Δl_h. Based upon a careful error analysis of PB, it is important to reveal the true character of it with high fidelity as an evidence of the hypothesis regulated by the modified Bragg law and BD in the present work.

V. Confirmatory Experiment

The four evidences mentioned in *Introduction*, namely the detection of PB in heavier crystals of InAs, GaSb and InSb than Ge provide a good test for the theory presented. They should be repeated if possible, at low temperature, because the occurrence of PB in those crystals has not yet been observed in spite of great expectation.

In order to examine the temperature effect on PB, it is desirable to use $\Delta(t)$ of reciprocal PCRRA. As stated in the section II, the inequality of $0 \leq \Delta(t) \leq 1$ in the temperature range from zero degree Kelvin to the melting point qualitatively expresses the temperature dependences of the rate of the recoil reflection. Generally, the D-W factor $D(t)$ quantitatively represents the fraction of the recoil-free reflection[25-28] and the cofactor of 1-$D(t)$ the fraction of the recoil reflection known as the thermal diffuse scattering in the total reflection

$$D(t) + \{1 - D(t)\} = 1 \tag{25}$$

closely relevant to the Bragg law in eq. (7).[21,40] Therefore, to discuss quantitatively the temperature dependence of PB, 1-$D(t)$ instead of $\Delta(t)$ could be effectively used.

The temperature variations of $D(t)$, 1-$D(t)$ and $\Phi(t)$ in eq. (1) for Si[21] with the high Debye temperature and for Al with the low value are tabulated in Table V. Both PB were observed at room temperature.[3,7] The function of $\Phi(t)$ is the commonly used function for all of materials.[32,37,41] Each individual of Si and Al is quite different from each other in D-W factor in dependence on the Debye temperature and the Bragg condition.

Generally, a crystal with the high Debye temperature is a high rigid crystal as stated. The reduced temperature, t in place of T, which is properly contracted by Θ_D, is a relevant measure of the degree of the crystal rigidity. It is shown in Table V (a) and (b) that t dependences of $\Phi(t)$, D(t) and 1-D(t) in Si with the higher Debye temperature are more insensitive than those with lower values. However, in common with not only Si and Al but also others materials, the higher the Miller indexes become, the more remarkable are D(t) and 1-D(t) coupled with those in eq. (1) vary.

As one of the confirmatory experiments, it is very important to observe the decreases of the intensities in all of PB in Si(hh0) following with roughly reductions by half in 1-D(t) depending on the temperature changes from 300K to 77K, since those in all of the Bragg peaks slowly increase by eq. (25) in Table V(a). In Al, both

$D(t)$ and 1-$D(t)$ greatly change over the temperature from 0K to 300K in Table V(b). It definitely indicates as a confirmation experiment that the integrated intensities of all PB in Al fade into quantum PB with decreasing temperature. As complementary event of PB in eq. (25), Nicklow *et al* reported in detail that the X-ray reflection intensities of Al increase with decreasing temperature, not only in (h00) but also (hh0) and (hhh), together with the increase of h.[42] The fade-ins in the Bragg peaks in Al(h00) with decreasing temperature[30,42] in eq. (25) qualitatively show good agreement with the result of ME in Fig. 2, in spite of the presence of the factor "*one fourth*" instead of $\sin^2\theta_B(\leq 1]$ in D-W factor of ME.[25,27,28] It suggests as test experiments that all of PB in not only Si and Al but also other all crystals resulting from the multiple recoil reflections should fade out in response to the decrease of 1-$D(t)$ with decreasing temperature. Consequently, it is considered that, although there is a large or small scale in temperature dependence of variations of PB due to the high or low Debye temperature, patterns of the Bragg peak observed at high temperature fade in with decreasing temperature but inversely those of PB fade out into quantum PB as a limit at 0K respectively.

The value of $D(0)$ due to the zero point vibration caused by the quantum effect is important at low temperatures. Considering the magnitude of 1-$D(0)$ $\geq$0.02, which is nearly equal to about half value of the minimum one of 1-$D(0.433)$=0.0392 of Si in Table V(a), it indicates that all of the PB strongly survives as the *quantum* PB due to the zero point vibration down to the absolute zero point, within a limitation of $\Delta(0)\neq 0$, for an imperfectly rigid crystal. Therefore, the observation of quantum PB, implying the complete absence of the elastic reflection in X-ray scattering is very interesting is an important test for validation experiments. Then, it is reasonable to expect that all of PB fade into quantum PB at very low temperature.

In our work, fundamental accounts of the particulars of PB, including PCRRA and experimental confirmations and understandings of the mechanism of the new beat formation, still remain to be carried out. They are not the main purpose in this work. The principle of the formation of beat from the multiple waves from more than two waves in X-ray is simply developed from the general physical viewpoint, independently of DTXD. The results encourage us to propose straightforward experiments to test the theory and to characterize the nature of the beats, apart from the old framework of PB.

Acknowledgements

The author would like cordially thanks to Dr M. Yoshizawa of Saitama Institute of Technology. for an offer of the unpublished data and useful discussion. He is also indebted to Prof. H. Kobayakawa of Nagoya University and Prof. Y. Hasegawa of Osaka City University ret., for useful suggestion and essentially helpful discussion.

Appendix I. On the principle of the equipartition of the recoil energy

Prior to ME, the analysis of the kinematics of γ-ray absorption in the nuclear physics was usually carried out for the case of a free atom. This is based on the fundamentally sound concept that the energies involved in nuclear reactions are so much larger than the energies of chemical binding that the atom may well be thought of as a free atom when analyzing nuclear events. However, it is possible to obtain Bragg reflection only for a

crystal, which is formed by a set of the tightly binding atoms, not free atoms. Therefore, the use of eq. (2) has been unreasonable in the solid-state physics. It is very important to introduce the recoil energy shared by all constituent atoms based upon the principle of the equipartition of it.

Let us consider a crystal of N atoms with the mass of m, into which the recoil velocity v is assumed to be equally parted. The absorbing atoms are assumed to be moving with velocities u_l at l site, so that the linear momentum of the system before absorption of the photon comprises $m\sum_{l=1}^{N} u_l$ and E_0/c is the X-ray photon momentum, which is assumed incident in the z-direction. After the absorption of X-ray photon, the linear momentum of the system is the excited atom plus $m\sum_{l=1}^{N}\left(u_{l//}+v/N\right)$ based upon the principle of the equipartition of the recoil energy. From the conservation of the linear momentum of the system, equating the components of momentum before and after the absorption of X-ray photon yields

$$m\sum_{l=1}^{N} u_{l//}+\frac{E_0}{c}=m\sum_{l=1}^{N}\left(u_{l//}+\frac{v}{N}\right) \qquad \text{(I-1)}$$

$$m\sum_{l=1}^{N} u_{l\perp}=m\sum_{l=1}^{N} u_{l\perp}, \qquad \text{(I-2)}$$

where the sign of // is parallel to z-direction and $\perp$ perpendicular to that. It follows from eq. (I-1) and (I-2) that the recoil momentum is given by

$$\frac{mv}{N}=\frac{1}{N}\cdot\frac{E_0}{c}=\frac{1}{N}\cdot\frac{h}{\lambda_0}, \qquad \text{(I-3)}$$

where $E_0 = hc/\lambda_0$. The recoil velocity is independent of the initial velocity of the atom. Let us consider the conservation of energy. Before the absorption of X-ray photon, the system consists of the energy of X-ray photon E_0 and the kinetic energy of the crystal as $(m/2)\sum_{l=1}^{N}\left(u_{l//}^2+u_{l\perp}^2\right)$. After the absorption, it consists of an excited state with the energy E_e and its kinetic state including the recoil velocity. Similarly, equating the energies before and after the absorption of X-ray photon yields:

$$E_0+\frac{m}{2}\sum_{l=1}^{N}\left(u_{l//}^2+u_{l\perp}^2\right)=E_e+\frac{m}{2}\sum_{l=1}^{N}\left\{\left(u_{l//}+\frac{v}{N}\right)^2+u_{l\perp}^2\right\}. \qquad \text{(I-4)}$$

By using eq. (I-3), the difference between E_0 and E_e from eq. (I-4) is given by

$$\delta E=E_e-E_0=-\frac{1}{2}\cdot\frac{mv^2}{N}-\frac{mv}{N}\sum_{l=1}^{N}u_{l//}\,.$$

$$=-E_R-\frac{E_0}{Nc}\sum_{l=1}^{N}u_{l//}\,, \qquad \text{(I-5)}$$

where the first term in eq. (I-5) is the recoil energy given in eq. (2) of

$$E_R=\frac{(mv)^2}{2Nm}=\frac{1}{2Nm}\cdot\left(\frac{E_0}{c}\right)^2. \qquad \text{(I-6)}$$

The second term in eq. (I-5) is the sum of the Doppler effect in each atom. A similar expression to the above could be derived in case of the emission of the photon.

If the recoil energy of (I-6) is valid independent of T, ME can be observed very easily even at room temperature. Therefore, it is reasonably apparent that the effective number N should be fixed through the temperature dependence of the rigidity of the crystal by the inverse PCRRA of

$$\Delta(T) = \frac{\delta(T)}{N}. \qquad \text{(I-7)}$$

Then, eq. (I-3) is expressed by

$$\Delta(T)mv = \frac{\delta(T)mv}{N} = \frac{\delta(T)}{N}\cdot\frac{E_0}{c} = \Delta(T)\frac{h}{\lambda}. \qquad \text{(I-8)}$$

The factor $\delta(T)$ might be expressed by something like the modified D-W factor. By use of eq. (I-7), the upper end of the common summation of l in eqs. (I-1), (I-2), (I-4) and (I-5) is replaced with $[N/\delta(T)]$, where [] is the Gauss' notation, which represents the greatest integer less than itself. For example, eq. (I-4) can be represented by

$$E_0 + \frac{m}{2}\sum_{l=1}^{[N/\delta(T)]}\left(u_{l//}^2 + u_{l\perp}^2\right) = E_e + \frac{m}{2}\cdot\sum_{l=1}^{[N/\delta(T)]}\left\{\left(u_{l//} + \frac{\delta(T)v}{N}\right)^2 + u_{l\perp}^2\right\},$$

whose recoil energy part of the right side becomes as

$$\frac{m}{2}\sum_{l=1}^{[N/\delta(T)]}\left\{\frac{\delta(T)}{N}v\right\}^2 = \frac{m}{2}\sum_{l=1}^{[N/\delta(T)]}\left\{\frac{\delta(T)}{Nm}\cdot\frac{E_0}{c}\right\}^2 = \frac{\delta(T)}{2Nm}\cdot\left(\frac{E_0}{c}\right)^2 = \frac{1}{2N_{PCRRA}(T)m}\cdot\left(\frac{E_0}{c}\right)^2,$$

where, from eq. (I-7),

$$[\Delta^{-1}(T)] = [\delta^{-1}(T)N] = N_{PCRRA}(T). \qquad \text{(I-9)}$$

The above expression satisfies the equipartition of the recoil energy.

Appendix II. On the bare beat formation formula-(i)

By using $\sin[\Theta + r\theta]\sin\theta/2 = (1/2)\{\cos[\Theta + (r\text{-}1/2)\Theta] - \cos[\Theta + (r+1/2)\theta]\}$, the summation of both sides of the following recursion formula from zero to n becomes

r=0: $\sin\Theta \quad \sin\theta/2 = (1/2)\{\cos[\Theta - \theta/2] \quad -\cancel{\cos[\Theta + \theta/2]}\}$

r=1: $\sin[\Theta + \theta] \quad \sin\theta/2 = (1/2)\{\cancel{\cos[\Theta + \theta/2]} \quad -\cancel{\cos[\Theta + 3\theta/2]}\}$

. .

. .

. .

$r=n$-1: $\sin[\Theta + (n\text{-}1)\theta]\sin\theta/2 = (1/2)\{\cancel{\cos[\Theta + (n\text{-}1\text{-}1/2)\theta]} - \cancel{\cos[\Theta + (n\text{-}1+1/2)\theta]}\}$

+) $r=n$: $\sin[\Theta + n\theta]\sin\theta/2 = (1/2)\{\cancel{\cos[\Theta + (n-1/2)\theta]} - \cos[\Theta + (n+1/2)\theta]$

$$\left\{\sum_{r=0}^{n}\sin[\Theta + r\theta]\right\}\sin\theta/2 = (1/2)\{\cos[\Theta - \theta/2] - \cos[\Theta + (n+1/2)\theta]\}$$

$$= \sin\left[\Theta + \frac{n\theta}{2}\right]\sin\frac{(n+1)\theta}{2}.$$

Considering $\sin\frac{\theta}{2}\neq 0$ in $0<\theta<2\pi$, the following expression could be obtained to be

$$\sum_{r=0}^{n}\sin\left[\Theta+r\theta\right]=\frac{\sin\left[\Theta+\frac{n\theta}{2}\right]\sin\frac{(n+1)\theta}{2}}{\sin\frac{\theta}{2}}. \qquad \text{(II-1)}$$

Alternating series of eq. (II-1) could be expressed as

$$\sum_{r=0}^{n}(-1)^{r}\sin\left[\Theta+r\theta\right]=\frac{\sin\left[\Theta+\frac{n(\theta+\pi)}{2}\right]\sin\frac{(n+1)(\theta+\pi)}{2}}{\sin\frac{\theta+\pi}{2}}. \qquad \text{(II-2)}$$

Eqs (II-1) and (II-2) represent the basic formulas of the bare beat formation by multiple superposition of the transmitted and diffracted photons as a simple algebraic sum, in utter disregard of the probability distribution of the transmitted and reflected photons.

Appendix III. On the bare beat formation formula-(ii) from the formula-(i)

The following finite direct product is expanded as a series of

$$2^{n}\prod_{r=1}^{n+1}\sin\left(\theta+\frac{r-1}{n+1}\pi\right)=2^{n}\prod_{r=1}^{n+1}\frac{1}{2i}\cdot\left\{e^{i\left(\theta+\frac{r-1}{n+1}\pi\right)}-e^{-i\left(\theta+\frac{r-1}{n+1}\pi\right)}\right\}$$

$$=2^{n}\prod_{r=1}^{n+1}\frac{1}{2i}\cdot\left\{\frac{e^{i\frac{r-1}{n+1}2\pi}\cdot e^{i2\theta}-1}{e^{i\frac{r-1}{n+1}\pi}\cdot e^{i\theta}}\right\}=2^{n}\cdot\left(\frac{1}{2i}\right)^{n+1}\cdot\left(e^{-i\frac{n}{2}\pi}\cdot e^{-i(n+1)\theta}\right)\cdot\prod_{r=1}^{n+1}\left(\omega_{r-1}\cdot e^{i2\theta}-1\right)$$

$$=(-1)^{n}\cdot e^{-i(n+1)\theta}\cdot\left(\frac{1}{2i}\right)\cdot\left\{\Omega_{n+1}\cdot\left(e^{i2\theta}\right)^{n+1}+(-1)^{1}\cdot\Omega_{n}\cdot\left(e^{i2\theta}\right)^{n}+\cdots\right.$$
$$\left.+(-1)^{n}\cdot\Omega_{1}\cdot\left(e^{i2\theta}\right)+(-1)^{n+1}\right\}, \qquad \text{(III-1)}$$

where $i^2 = -1$. By using

$$\omega_{s}=\left(e^{i2\pi}\right)^{\frac{s}{n+1}}=(1)^{\frac{s}{n+1}}, \qquad (0\le s\le n) \qquad \text{(III-2)}$$

as the $(n+1)$-th root of 1, the polynomial of x^{n+1} -1 could be resolved into the factors as:

$$x^{n+1}-1=(x-\omega_{0})(x-\omega_{1})\cdots(x-\omega_{n})$$
$$=x^{n+1}+(-1)^{1}\Omega_{1}x^{n}+(-1)^{2}\Omega_{2}x^{n-1}+\cdots+(-1)^{n}\Omega_{n}x+(-1)^{n+1}\Omega_{n+1}, \qquad \text{(III-3)}$$

in which

$$\Omega_{s}=\sum_{0\le j_{1}<\cdots<j_{s}\le n}\omega_{j_{1}}\omega_{j_{2}}\cdots\omega_{j_{s}}. \qquad (1\le s\le n). \qquad \text{(III-4)}$$

From the comparison of the coefficients in the both sides of eq. (III-3), the next expressions are obtained to be

$$\begin{cases}\Omega_{s}=0 & (1\le s\le n)\\ \Omega_{n+1}=(-1)^{n}.\end{cases} \qquad \text{(III-5)}$$

Using eqs. (III-2), (III-4) and (III-5), eq. (III-1) successively becomes as follows:

$$=(-1)^{n}\cdot\frac{e^{-i(n+1)\theta}}{2i}\cdot\left\{(-1)^{n}\cdot e^{i2(n+1)\theta}+(-1)^{n+1}\right\}=\frac{1}{2i}\left\{e^{i(n+1)}-e^{-i(n+1)}\right\}$$

$$\therefore \sin(n+1)\theta = 2^n \prod_{r=1}^{n+1} \sin\left(\theta + \frac{r-1}{n+1}\pi\right) = 2^n \sin\theta \prod_{r=1}^{n} \sin\left(\theta + \frac{r}{n+1}\pi\right). \qquad \text{(III-6)}$$

References

1. N. Kato and A. R. Lang: Acta Cryst. **12** (1959) 787.
2. R. A. Duckett and A. R. Lang: J. Cryst. Growth **18** (1973) 135.
3. T. Saka and N. Kato: Acta Cryst **A42** (1986) 469.
4. A. R. Lang and Z. H. Mai: Proc. R. Soc. London Ser. A **368** (1979) 313.
5. T. Takama, K. Tsuchiya, K. Kobayashi and S. Sato: Acta Cryst. **A46** (1990) 514.
6. A. Zarka: Bull. Soc. Fr. Mineral Cristallogr. **92** (1969) 160.
7. T. Takama, K. Kobayashi and S. Sato: Transaction Jpn In Metals **23** (1982) 153.
8. T. Takama and S. Sato: Phil. Mag. **45** (1982) 615.
9. T. Takama, K. Kobayashi, M. Hyugaji, O. Nittono and S. Sato: Jpn. J. Appl. Phys. **23** (1984) 11.
10. K. Kobayashi, T. Takama, S. Tohno and S. Sato: Jpn. J. Appl. Phys. **27** (1988) 1793.
11. M. Yoshizawa, T. Kawamura, K. Ehara, H. Sugawara, T. Nakajima, T. Fukamachi and K. Hayakawa: Photon Factory Activity Report #4 (1986) p.161 (ed. by N. Sakabe *et al.*)
12. M. Yoshizawa, T. Kawamura, K. Ehara, T. Nakajima, H. Sugawara, T. Fukamachi and K. Hayakawa: Acta Cryst. **A43** (1986) Suppl. C262 15.4-2.
13. M. Yoshizawa: (Doctor thesis, Univ. of Tokyo, 1996).
14. K. Kobayashi, T. Takama, and S. Tohno: Jpn. J. Appl. Phys. **27** (1981) 1377.
15. T. Takama and S. Sato: Jpn. J. Appl. Phys. **20** (1981) 1183.
16. K. A. Gschneidner, Solid State Physics (Academic Press, New York & London, 1964) **16** p. 368.
17. R. L. Moessbauer: *Z. Physik* **151** (1958) 124.
18. R. L. Moessbauer: Naturwiss. **22** (1958) 538.
19. R. L. Moessbauer: Z. Naturforsch. **14a** (1959) 211.
20. W. M. Visscher: Ann. Phys. **9** (1960) 194.
21. T. Nakajima: J. Low Temp. Phys. **128** (2002) 9 and Physica **B329-333** (2003) 410.
22. R. V. Pound and G. A. Rebka: Jr., Phys. Rev. Letters **3** (1959) 554.
23. R. L. Moessbauer: Rev Mod Phys **36** (1964) 410.
24. R. H. Herber: *McGraw-Hill Encyclopedia of Physics* (2nd ed. McGraw-Hill Inc., New York etc. 1993) p. 814.
25. H. Frauenfelder: *The Moessbauer Effect* (W. A. Benjamin Inc. New York, 1962) Chap. 2, p. 14
26. S. Nakajima: *Solid State Physics* II (Iwanami Shoten, Tokyo, 1972) p. 22 [in Japanese]
27. J. van Kranendonk: Proc. VIIth Intern. Con. Low Temp. Phys. (G. M. Graham and A. C. Hollis Hellet (eds.), Univ. Tront Press, 1961) **9-20**, p. 9.
28. K. Yoshida: *Jisei* (*Magnetism*) (Asakura-shoten, Tokyo, 1972) p. 19 [in Japanese].
29. H. Kitamura, *Insertion Device Handbook* p. 59 (KEK Report 89-24 March 1990). Using the beam size of 0.2mm square at the down-stream of 27.0m from the light source point in BL-6, the effective number of the incident photon flux of n is obtained to be n = photon density of $1.84 \cdot 10^{13}$ (photons/$s \cdot$mrad$^2 \cdot 0.1\%$ band width) $\times$ $(0.2/27.0)^2$ (mrad^2)= $1.09 \cdot 10^9$ (photons/s$\cdot 0.1\%$ band width).
30. C. Kittel: *Introduction to Solid State Physics* (6th ed. John Wiley & Sons, Inc., New York, Chichester, Brisbane, Tronto, Singapore, 1986) p. 34 and p. 601.
31. J. J. Sakurai: *Advanced Quantum Mechanics* (Addison-Wesley Publishing Company, New York, Ontario, Amsterdam, Bonn, Sydney, Tokyo, Paris, 1967) p. 47
32. S. Miyake: *Diffraction of X-rays.* (Asakura-shoten, Tokyo, 1969)p. 149 and p. 222 [in Japanese]
33. M. Yoshizawa: private communication
34. P. A. M. Dirac: *The Principles of Quantum Mechanics* (Oxford at the Clarendon Press, 1958) p. 7.

35. G.. Borrmann: Z. Phys. **127** (1950) 297.

36. H. N. Campbell: J. Appl. Phys. **22** (1951) 1139.

37. B. D. Cullity, *Elements of X-ray Diffraction* (2nd ed. Addison-Wesley Publishing Co. Inc., Reading, Massachusetts, U. S. A., 1978) p. 257 and Appendix 15

38. A. T. Forrester, R. A. Gudmundsen and P. Q. Johnson: Phys. Rev. *99* (1955) 1691.

39. The sequence of numbers $\{\sqrt[l]{l}\}(l \geq 3)$ is monotonically decreasing with a lower bound of 1 as $\sqrt[l]{l} > \sqrt[l+1]{l+1} > 1(l \geq 3),$ because the function of $f(x)=\sqrt[x]{x}(x > 0)$ is monotone decreasing one over a range of $e \leq x < \infty$ that takes the maximum value of $\sqrt[e]{e}$ (= 1.444667861・・・) at $x=e$ (e=2.7182818・・・).

40. For example, Leonid V. Azaroff: *Elements of X-ray Crystallography* (McGraw- Hill Book Co., New York, 1968) p. 234.

41. A. Guinier: *X-ray Diffraction* (Dover Publications Inc., New York, 1994) p. 189.

42. R. M. Nicklow and R. A. Young: Phys. Rev. **152** (1966) 591.

Table I. Typical example of the observed Pendelloesung Beats.

Materials	Atomic number Z*	Atomic Weight M*	Debye-Waller Factor		Ref.
			$\Theta_D(K)$	$E_c\ (keV)$	
Hexamethaline Tetramine $N_4(CH_2)_6$	3.4	6.37			2
C (diamond)	6	12.011	1874	24.5	4, 5
LiF	6	12.970	732	15.9	1
Dolomite $MgCa(CO_3)_2$	9.2	18.440			6
Quartz SiO_2	10	20.028	470	15.8	1
Al	13	26.982	390	16.7	7
Si	14	28.086	692	22.7	1, 3
Cu	29	63.546	310	22.9	8
Zn	30	65.39	237	20.3	9
InP	32	72.897	321	25.0	10
GaAs	32	72.323	344	25.7	11-14
Ge	32	72.61	403	27.9	15
InAs	41	94.871	249	25.14	None
GaSb	41	95.737	266	26.10	None
InSb	50	118.285	203	25.35	None

Effective atomic number Z* and atomic weight M* are temporally defined by

$$Z^* = \sum_i n_i Z_i \Big/ \sum_i n_i \quad \text{and} \quad M^* = \sum_i n_i M_i \Big/ \sum_i n_i ,$$

where n_i is number of the i element for compounds. The quantity E_C of the 4-th column is defined by $(mc^2 k_B \Theta_D / 3)^{1/2}$, which the weighted geometrical mean between mc^2 and $k_B\Theta_D$,[21] where Θ_D is cited from the reference 16.

Table II. Data of the sample used for measurement of PB in GaAs.[11-13]

Lattice constant(nm)	Sample size thickness×area	N(atoms)	E_0 (keV) Ga K	λ_0 (nm)	ω_0 (rad/sec)
0.56419	$200\mu m \times 10^2 cm^2$	$8.91 \cdot 10^{20}$	10.268	0.1207	$1.56 \cdot 10^{19}$

Table III. Various physical quantities of GaAs determined from the experiments.

l eq. (9)	$2E_R$(keV) eq. (4)	$\Delta\omega$ (rad/sec) eq. (8)	$l\Delta\omega$ (rad/sec) eq. (8)	$N_{eff}(300K)$ eq. (4)
155,933	$11.41\cdot10^{-18}$	$2.19\cdot10^{8}$	$3.42\cdot10^{13}$	$1.42\cdot10^{11}$

λ_{t_0} (m) for GaAs	τ (sec) eq. (11)	$(\Delta\lambda/\lambda)_D$ eq. (12)	$\delta(300K)$ eqs.(8)&(12)	$\Delta(300K)$ eqs. (8)&(12)	$\Delta\lambda$ (m) eq. (12)
$110.08\cdot10^{-6}$	$3.67\cdot10^{-13}$	$2.19\cdot10^{-6}$	$6.26\cdot10^{9}$	$7.03\cdot10^{-12}$	$2.64\cdot10^{-16}$

$(\Delta\lambda/\lambda_0 = -\Delta\omega/\omega_0$ from $\omega = ck)$

Table IV. Pascal's triangle used for the Borrmann fan and the Binomial Distribution in Fig 4.

	${}_lC_r=\binom{l}{r}=\frac{l!}{(l-r)!r!}$	$d^{l-r}t^r=(1/2)^l$
l=0	${}_0C_0=1$	$(1/2)^0=1$
l=1	${}_1C_0=1$ ${}_1C_1=1$	$(1/2)^1=1/2$
l=2	${}_2C_0=1$ ${}_2C_1=2$ ${}_2C_2=1$	$(1/2)^2=1/4$
l=3	${}_3C_0=1$ ${}_3C_1=3$ ${}_3C_2=3$ ${}_3C_3=1$	$(1/2)^3=1/8$
l=4	${}_4C_0=1$ ${}_4C_1=4$ ${}_4C_2=6$ ${}_4C_3=4$ ${}_4C_4=1$	$(1/2)^4=1/16$
l=5	${}_5C_0=1$ ${}_5C_1=5$ ${}_5C_2=10$ ${}_5C_3=10$ ${}_5C_4=5$ ${}_5C_5=1$	$(1/2)^5=1/32$
	…….	

The binomial coefficient satisfy the following relations:

${}_lC_r={}_lC_{l-r}$ (from the bilateral symmetry)

and

${}_lC_r={}_{l-1}C_{r-1}+{}_{l-1}C_r$ (from the Pascal's formula).

Table V. Temperature variations of D(t) and 1-D(t) for Si and Al.

By using the energy dispersive Bragg law of $dE_0 \sin\theta_B = 0.6199$, D-W factor in eq. (1) is rewritten as follows:

$$D(t) = \exp\left\{-\left(E_0 \sin\theta_B / E_C\right)^2 \Phi(t)\right\} = \exp\left\{-\left(d_C/a\right)^2 (h^2+k^2+l^2)\Phi(t)\right\},$$

where a is the lattice parameter of $1/d^2 = (h^2+k^2+l^2)/a^2$.

(a) $D(t)$=exp{- $5.0572 \cdot 10^{-3} h^2 \Phi(t)$} and 1-$D(t)$ for Si(hh0), where a=0.5431nm.

(hh0).	t	0(0K)	0.111(77K)	0.433(300K)
	$\Phi(t)$	1	1.073	1.978
(220).	$D(t)$	0.9800	0.9785	0.9608
	1-$D(t)$	0.0200	0.0215	0.0392
(440).	$D(t)$	0.9223	0.9168	0.8521
	1-$D(t)$	0.0777	0.0832	0.1479
(660).	$D(t)$	0.8336	0.8225	0.6976
	1-$D(t)$	0.1664	0.1775	0.3024

(b) $D(t)$=exp{- $0.0252 h^2 \Phi(t)$} and 1-$D(t)$ for Al(hhh), where a=0.4050nm.

(hhh).	t	0(0K)	0.197(77K)	0.769(300K)
	$\Phi(t)$	1	1.251	3.221
(111).	$D(t)$	0.9751	0.9690	0.9220
	1-$D(t)$	0.0249	0.0310	0.0780
(222).	$D(t)$	0.9041	0.8815	0.7228
	1-$D(t)$	0.0959	0.1185	0.2772
(333).	$D(t)$	0.7971	0.7530	0.4817
	1-$D(t)$	0.2029	0.2470	0.5183

Figure captions

Fig 1. The recoil energy loss E_R (meV) versus the photon energy E_0 (keV) for all free single atom with some atomic weights of M_a=0.004kg/mol (He), 0.012kg/mol (C), 0.072kg/mol (Ge), 0.100kg/mol and 0.200kg/mol. PB has been observed in a region within *abcd* from the range over 10keV ≤ E_0 ≤ 60keV and 0.74meV≤E_R≤ 161meV.

Fig 2. The effective resonance absorption cross section per ^{191}Ir nucleus, for the absorber crystal at 88K and the source temperature given by the abscissa. Experimental data are reproduced from the reference 17. Here, the Debye temperature Θ_D of 318K is used at 88K. The Debye temperature of Ir exceptionally changes over a range from 228K at 298K to 425 ± 5K at 0K[16], which promotes the absorption cross section.

Fig 3. Schematic diagram of the multiple Bragg reflections of an incident X-ray photon with the Bragg angle of θ_B in the crystal net plane with the discrete spacing of d_{hkl}, in order to derive the modified Bragg law due to the recoil reflection based upon the corpuscular nature of the light.

Fig 4. Schematic diagram of the multiple reflections of an incident X-ray photon with the Bragg angle of θ_B in the crystal net plane with the discrete spacing of d_{hkl}. The triangle in the Laue case is called by the name of the Borrmann fan in DTXD.

Fig 5. Schematic diagrams of a step of the multiple reflections of an photon used for counting the optical paths.

(a) The alternative of the G-wave (*G*) paralleled on the first diffracted photon or O-wave (*O*) paralleled on an incident photon in the two wave approximation in DTXD.

(b) The alternative of the flexion (*d*) or the beeline (*t*) at each reflection point used for counting the number of reflection.

Fig 6. The curves of (a) l_h=1, (b) l_h=2, (c) l_h=3, (d) l_h=4, (e) l_h=19, (f) l_h=20, (g) l_h=29 and (h) l_h=30 reproduced from eqs. (22a) and (22b) are shown by plotting over an angular range of $-25^\circ \leq \Delta\omega t \leq 385^\circ$. For form's sake, *l* in Fig. 4 is replaced by l_h.

Fig 7(a). l_h=9 and (b) l_h=10.

The function of $\sin(l_h+1)\Delta\omega t \ \mathrm{cosec}\,\Delta\omega t \left\{= 2^{l_h}\prod_{r=1}^{l_h}\sin\left(\Delta\omega t + \frac{r\pi}{l_h+1}\right)\right\}$ in eq. (22a), together with $\sin(l_h+1)\Delta\omega t \left(= 2^{l_h}\prod_{r=0}^{l_h}\sin\left(\Delta\omega t + \frac{r\pi}{l_h+1}\right)\right)$, is plotted against angular region of $-25^\circ \leq (l_h+1)\Delta\omega t \leq 385^\circ$. In these curves, the intrinsic sine functions of $\sin(l_h+1)\Delta\omega t$ (l_h=9 and 10) are modulated

in amplitude and frequency by cosec $\Delta\omega t$.

Fig 8. The optical paths and the transmitted and diffracted photons obtained using the way of Fig 5(b) in the multiple reflections of an incident photon.

(a) the mono-layer crystal (l=1).

(b) the double layer crystal(l=2).

(c) the triple layer crystal (l=3).

Fig 9. Some typical patterns of intrinsic PB reproduced from eq. (16) over a time range of $0 \le t \le 4.5$ in the case of $\omega_0 = 20$rad/s, $\Delta\omega = -1$ rad/s and A=1.

(a) An incident beam of $\psi(t) = \sin 20t$.

(b) $\psi_{trans}^{l=3}(t) = \left(\frac{1}{2}\right)^3 \sum_{p=0}^{1} \binom{3}{2p} \sin[20 - 2p]t = \frac{1}{8}\sin 20t + \frac{3}{8}\sin 18t$

(c) $\psi_{diff}^{l=3}(t) = \left(\frac{1}{2}\right)^3 \sum_{p=0}^{1} \binom{3}{2p+1} \sin[20 - (2p+1)]t = \frac{3}{8}\sin 19t + \frac{1}{8}\sin 17t$.

(d) For comparison, $\psi_{trans}^{l=3}(t)$ and $\psi_{diff}^{l=3}(t)$ are superimposed one over another.

(e) $\psi_{trans}^{l=4}(t) = \left(\frac{1}{2}\right)^4 \sum_{p=0}^{2} \binom{4}{2p} \sin[20 - 2p]t = \frac{1}{16}\sin 20t + \frac{6}{16}\sin 18t + \frac{1}{16}\sin 16t$

(f) $\psi_{diff}^{l=4}(t) = \left(\frac{1}{2}\right)^4 \sum_{p=0}^{1} \binom{4}{2p+1} \sin[20 - (2p+1)]t = \frac{4}{16}(\sin 19t + \sin 17t) = \frac{1}{2}\sin 18t \cos t$

(g) For comparison, $\psi_{trans}^{l=4}(t)$ and $\psi_{diff}^{l=4}(t)$ are superimposed one over another.

Fig 10 (a) and (b) $\psi_{+}^{l=3}$ and $\psi_{+}^{l=4}$ reproduced from eqs. (17) and (18), respectively, over a time range of $0 \le t \le 4.5$ in the case of $\omega_0 = 20$ rad/s, $\Delta\omega = -1$ rad/s and A=1.

(a) $\psi_{+}^{l=3}(t) = 2 \sin 19t \cos t$ in eq. (17).

(b) $\psi_{+}^{l=4}(t) = 4 \sin 18t \sin(-t + \pi/3) \sin(-t + 2\pi/3)$ in eq. (18), in which the function of f(t)= 4 sin (-t+ π /3) sin (-t+2 π /3) is shown in Fig 5(b).

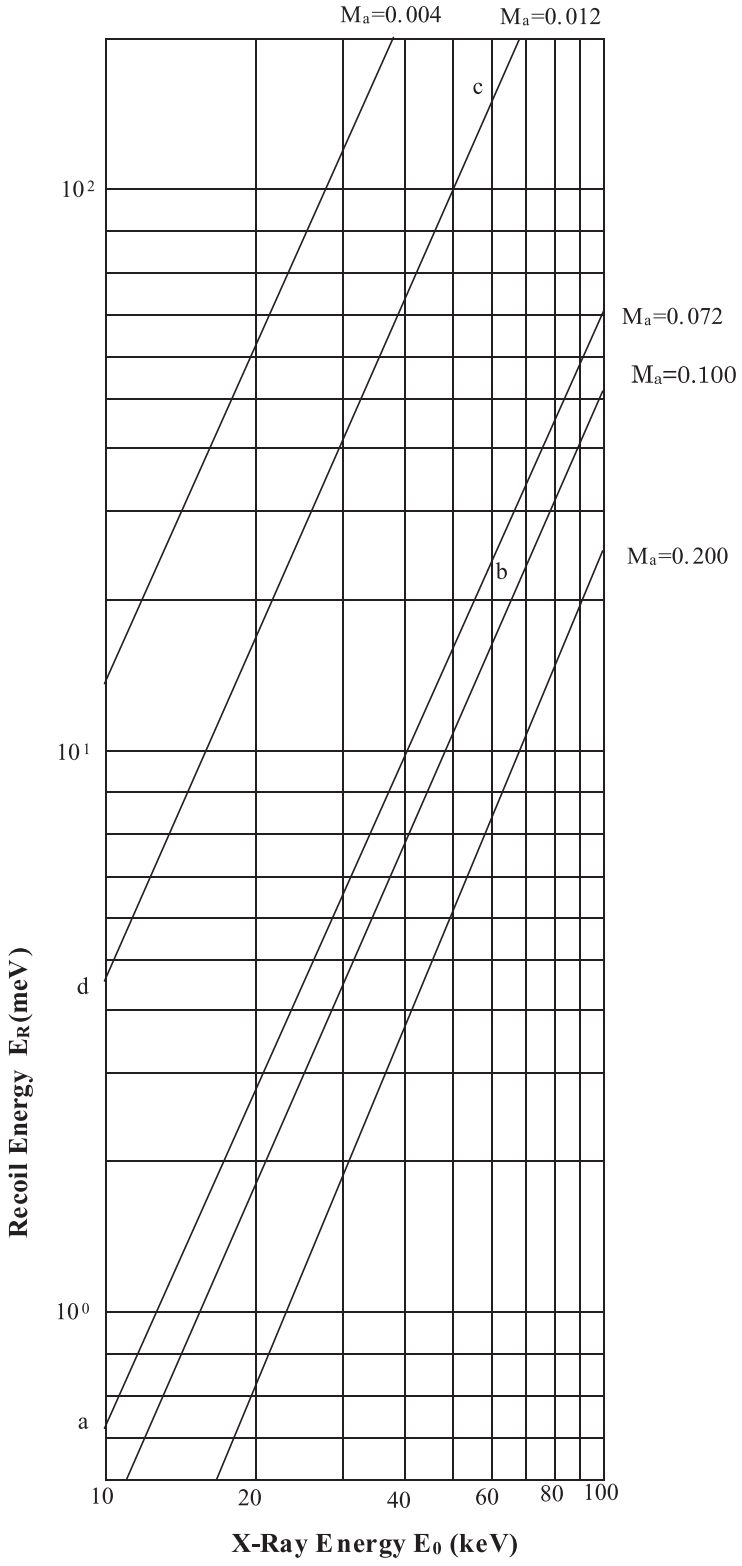

Fig 1. The recoil energy loss E_R (meV) versus the photon energy E_0 (keV) for all free single atom with some atomic weights of M_a=0.004kg/mol (He), 0.012kg/mol (C), 0.072kg/mol (Ge), 0.100kg/mol and 0.200kg/mol. PB has been observed in a region within *abcd* from the range over 10keV ≤ E_0 ≤ 60keV and 0.74meV≤E_R≤ 161meV.

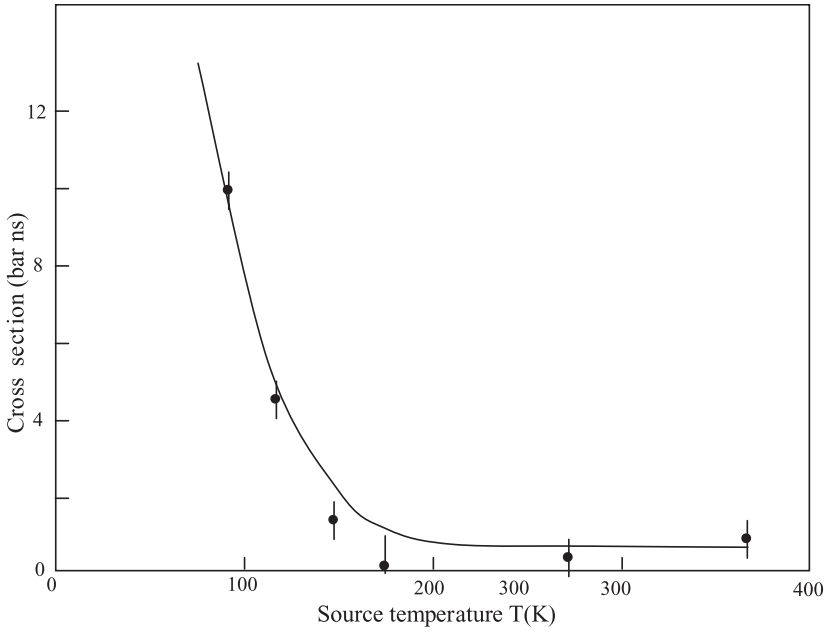

Fig 2. The effective resonance absorption cross section per ^{191}Ir nucleus, for the absorber crystal at 88K and the source temperature given by the abscissa. Experimental data are reproduced from the reference 17. Here, the Debye temperature Θ_D of 318K is used at 88K. The Debye temperature of Ir exceptionally changes over a range from 228K at 298K to 425 ± 5K at 0K[16], which promotes the absorption cross section.

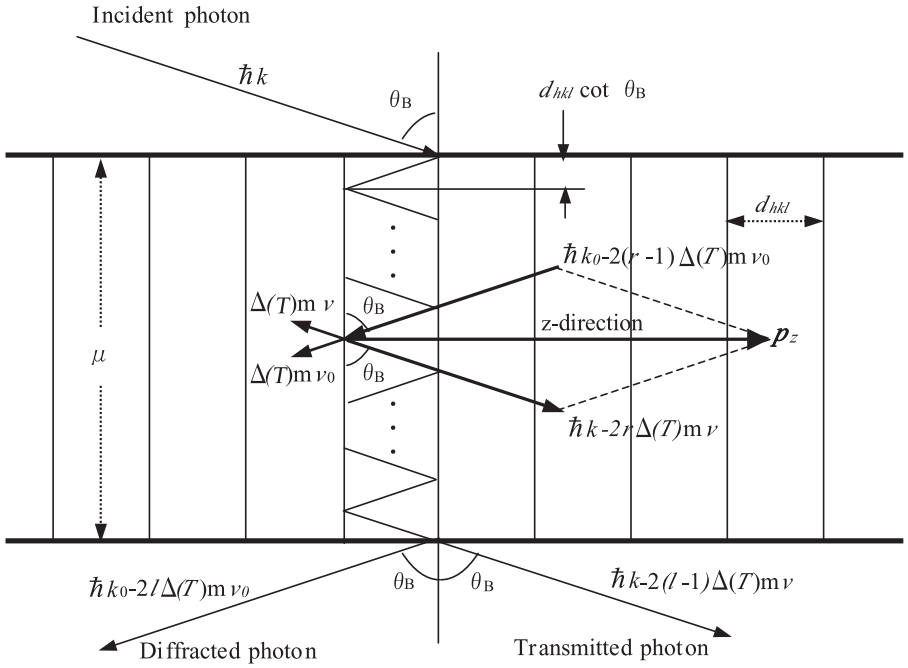

Fig 3. Schematic diagram of the multiple Bragg reflections of an incident X-ray photon with the Bragg angle of θ_B in the crystal net plane with the discrete spacing of d_{hkl}, in order to derive the modified Bragg law due to the recoil reflection based upon the corpuscular nature of light.

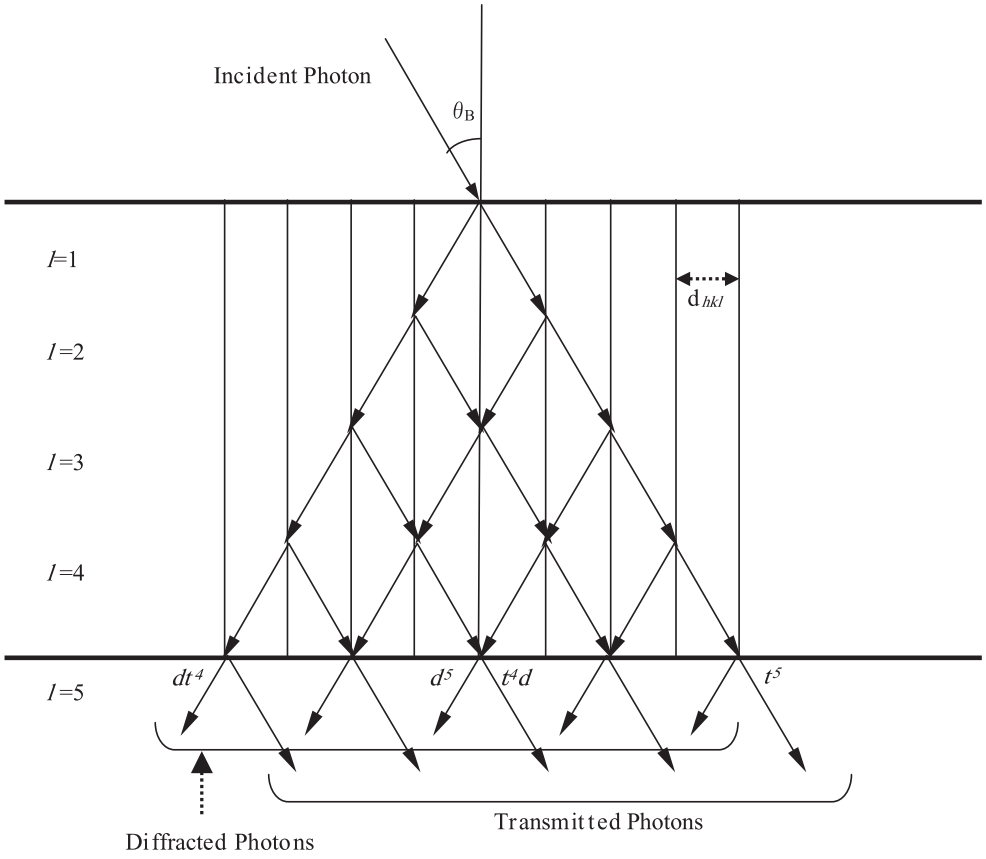

Fig 4. Schematic diagram of the multiple reflections of an incident X-ray photon with the Bragg angle of θ_B in the crystal net plane with the discrete spacing of d_{hkl}. The triangle in the Laue case is called by the name of the Borrmann fan in DTXD.

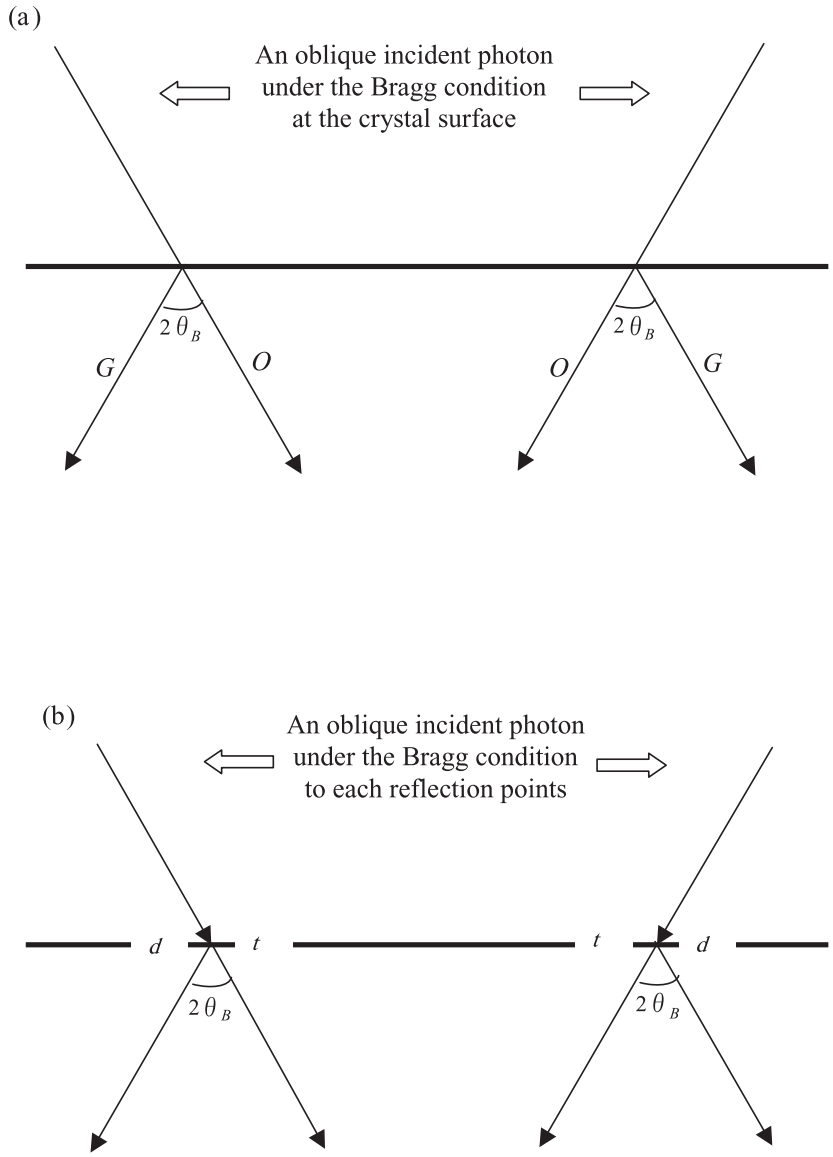

Fig 5. Schematic diagrams of a step of the multiple reflections of an photon used for counting the optical paths.

(a) The alternative of the G-wave (*G*) paralleled on the first diffracted photon or O-wave (*O*) paralleled on an incident photon in the two wave approximation in DTXD.

(b) The alternative of the flexion (*d*) or the beeline (*t*) at each reflection point used for counting the number of reflection.

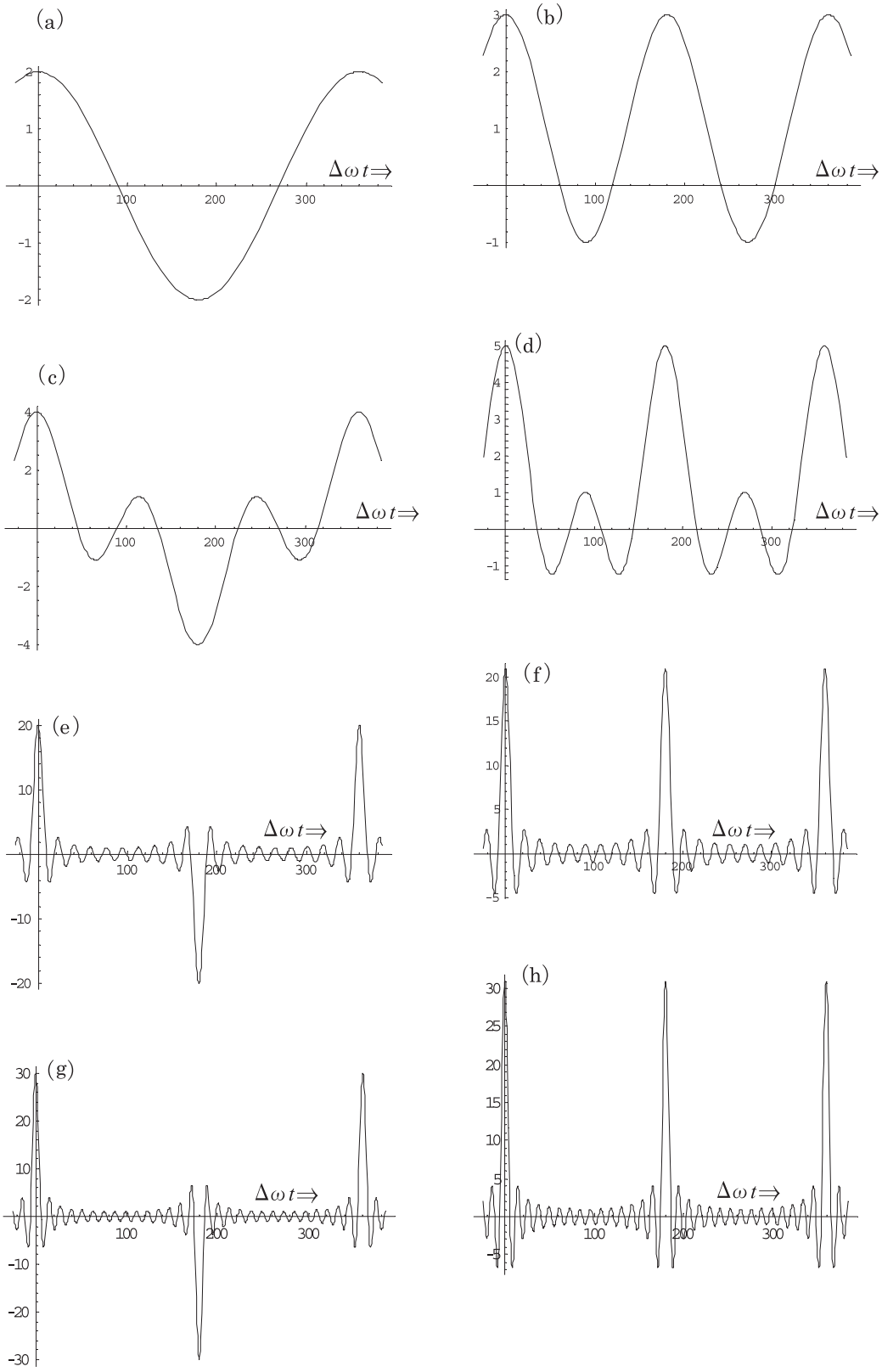

Fig 6. The curves of (a) l_h=1, (b) l_h=2, (c) l_h=3, (d) l_h=4, (e) l_h=19, (f) l_h=20, (g) l_h=29 and (h) l_h=30 reproduced from eqs. (22a) and (22b) are shown by plotting over an angular range of $-25^\circ \leq \Delta\omega t \leq 385^\circ$. For form's sake, l in Fig. 4 is replaced by l_h.

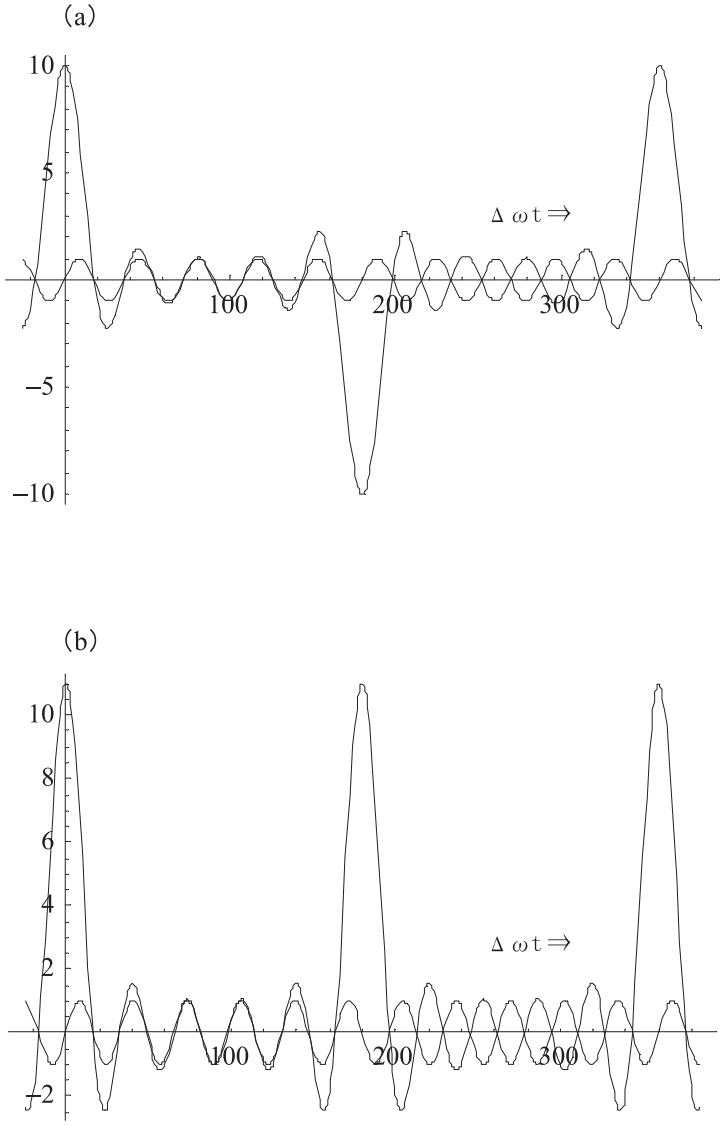

Fig 7(a). l_h=9 and (b) l_h=10.

The function of $\sin(l_h+1)\Delta\omega t \ \mathrm{cosec}\,\Delta\omega t \ \left\{= 2^{l_h}\prod_{r=1}^{l_h}\sin\left(\Delta\omega t + \frac{r\pi}{l_h+1}\right)\right\}$ in eq. (22a), together with $\sin(l_h+1)\Delta\omega t \left(= 2^{l_h}\prod_{r=0}^{l_h}\sin\left(\Delta\omega t + \frac{r\pi}{l_h+1}\right)\right)$, is plotted against angular region of -25° $\leq(l_h+1)\Delta\omega t \leq 385°$. In these curves, the intrinsic sine functions of $\sin(l_h+1)\Delta\omega t$ (l_h=*9* and *10*) are modulated in amplitude and frequency by $\mathrm{cosec}\,\Delta\omega t$.

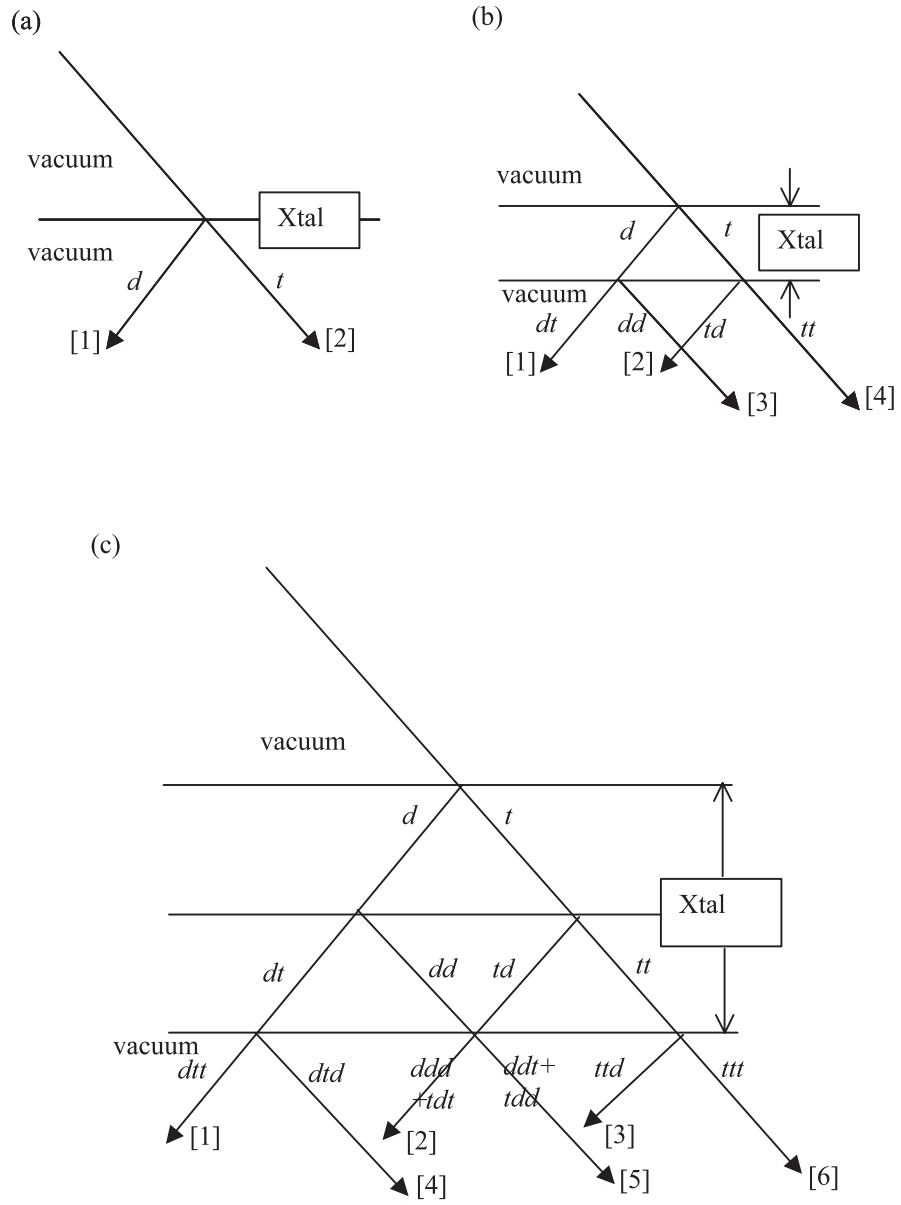

Fig 8. The optical paths and the transmitted and diffracted photons obtained using the way of Fig 5(b) in the multiple reflections of an incident photon.

(a) the mono-layer crystal (l=1).

(b) the double layer crystal(l=2).

(c) the triple layer crystal (l=3).

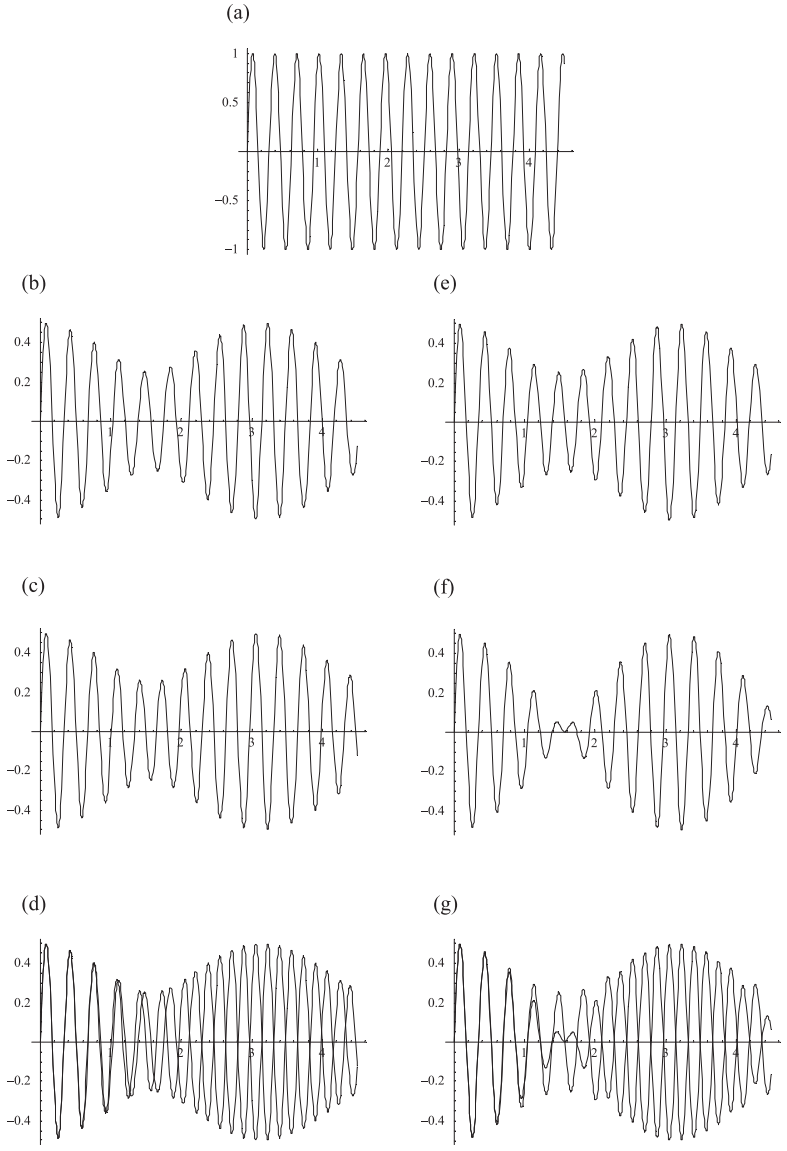

Fig 9. Some typical patterns of intrinsic PB reproduced from eq. (16) over a time range of $0 \le t \le 4.5$ in the case of $\omega_0 = 20$rad/s, $\Delta\omega = -1$ rad/s and $A=1$.

(a) An incident beam of $\psi(t) = \sin 20t$.

(b) $$\psi_{trans}^{l=3}(t) = \left(\frac{1}{2}\right)^3 \sum_{p=0}^{1} \binom{3}{2p} \sin[20 - 2p]t = \frac{1}{8}\sin 20t + \frac{3}{8}\sin 18t$$

(c) $$\psi_{diff}^{l=3}(t) = \left(\frac{1}{2}\right)^3 \sum_{p=0}^{1} \binom{3}{2p+1} \sin[20 - (2p+1)]t = \frac{3}{8}\sin 19t + \frac{1}{8}\sin 17t\,.$$

(d) For comparison, $\psi_{trans}^{l=3}(t)$ and $\psi_{diff}^{l=3}(t)$ are superimposed one over another.

(e) $$\psi_{trans}^{l=4}(t) = \left(\frac{1}{2}\right)^4 \sum_{p=0}^{2} \binom{4}{2p} \sin[20 - 2p]t = \frac{1}{16}\sin 20t + \frac{6}{16}\sin 18t + \frac{1}{16}\sin 16t$$

(f) $$\psi_{diff}^{l=4}(t) = \left(\frac{1}{2}\right)^4 \sum_{p=0}^{1} \binom{4}{2p+1} \sin[20 - (2p+1)]t = \frac{4}{16}(\sin 19t + \sin 17t) = \frac{1}{2}\sin 18t \cos t$$

(g) For comparison, $\psi_{trans}^{l=4}(t)$ and $\psi_{diff}^{l=4}(t)$ are superimposed one over another.

(a)

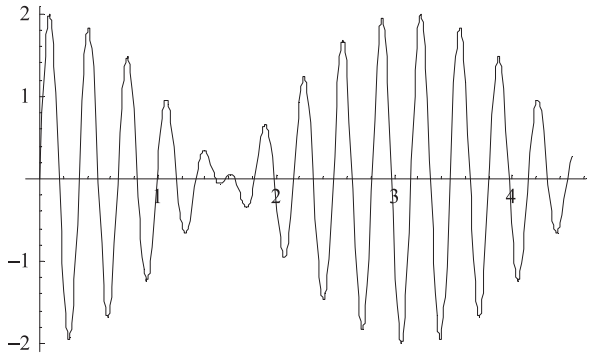

(b)

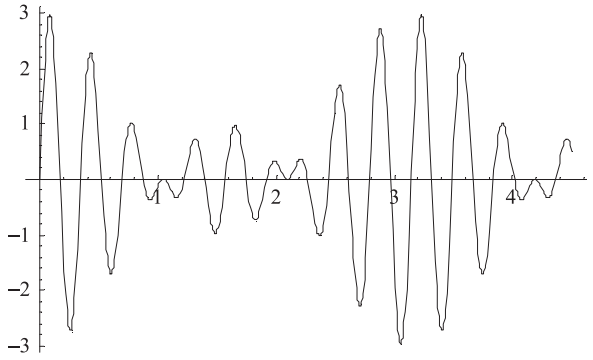

Fig 10 (a) and (b) $\psi_{+}^{l=3}$ and $\psi_{+}^{l=4}$ reproduced from eqs. (17) and (18), respectively, over a time range of $0 \leq t \leq 4.5$ in the case of $\omega_0 = 20$ rad/s, $\Delta\omega = -1$ rad/s and A=1.

(a) $\psi_{+}^{l=3}(t) = 2 \sin 19t \cos t$ in eq. (17).

(b) $\psi_{+}^{l=4}(t) = 4 \sin 18t \sin(-t.+ \pi /3) \sin (-t+2 \pi /3)$ in eq. (18), in which the function of f(t)= 4 sin (-t+ π /3) sin (-t+2 π /3) is shown in Fig 5(b).